

EXPERIMENTAL INVESTIGATION OF THE EFFECTS OF TIP GEOMETRY
ON THE FLOW AND LOSS CHARACTERISTICS IN A LINEAR TURBINE
CASCADE

A THESIS SUBMITTED TO
THE GRADUATE SCHOOL OF NATURAL AND APPLIED SCIENCES
OF
MIDDLE EAST TECHNICAL UNIVERSITY

BY

OZAN ALİCAN

IN PARTIAL FULFILLMENT OF THE REQUIREMENTS
FOR
THE DEGREE OF MASTER OF SCIENCE
IN
AEROSPACE ENGINEERING

JANUARY 2017

Approval of the thesis:

**EXPERIMENTAL INVESTIGATION OF THE EFFECTS OF TIP
GEOMETRY ON THE FLOW AND LOSS CHARACTERISTICS IN A
LINEAR TURBINE CASCADE**

submitted by **OZAN ALICAN** in partial fulfillment of the requirements for the degree of **Master of Science in Aerospace Engineering Department, Middle East Technical University** by,

Prof. Dr. Gülbin Dural Ünver _____
Dean, **Graduate School of Natural and Applied Sciences**

Prof. Dr. Ozan Tekinalp _____
Head of Department, **Aerospace Engineering**

Assoc. Prof. Dr. Oğuz Uzol _____
Supervisor, **Aerospace Engineering Dept., METU**

Examining Committee Members:

Assoc. Prof. Dr. Sinan Eyi _____
Aerospace Engineering Dept., METU

Assoc. Prof. Dr. Oğuz Uzol _____
Aerospace Engineering Dept., METU

Assoc. Prof. Dr. M.Metin Yavuz _____
Mechanical Engineering Dept., METU

Asst. Prof. Dr. Harika S. Kahveci _____
Aerospace Engineering Dept., METU

Asst. Prof. Dr. Sıtkı Uslu _____
Mechanical Engineering Dept., TOBB ETU

Date: 20.01.2017

I hereby declare that all information in this document has been obtained and presented in accordance with academic rules and ethical conduct. I also declare that, as required by these rules and conduct, I have fully cited and referenced all material and results that are not original to this work.

Name, Last Name: Ozan, Alican

Signature:

ABSTRACT

EXPERIMENTAL INVESTIGATION OF THE EFFECTS OF TIP GEOMETRY ON THE FLOW AND LOSS CHARACTERISTICS IN A LINEAR TURBINE CASCADE

ALİCAN, Ozan

M.Sc., Department of Aerospace Engineering

Supervisor: Asst. Prof. Dr. Oğuz UZOL

January 2017, 108 pages

In gas turbines, there are a number of factors causing efficiency decrease. When internal flow in turbomachines is considered, flow vortices are one of those factors. This study aims to investigate the main mechanisms behind the efficiency losses occurring due to Tip Leakage Vortex (TLV) in gas turbine rotor blades. Additionally, according to these mechanisms, two squealer tip geometries were applied to the turbine blades and the improvements were reported. This work is the experimental branch of an optimum tip geometry investigation and an optimum solution from different squealer geometries were tested and compared with the CFD-based investigations. In the scope of this work, experiments were planned as two cases; flat tip and squealer tips. These were named as “No Treatment” and “Treated Tip Cases” respectively. No Treatment case was considered as the reference case and Treated Tip cases’ results were compared to the reference. In the Treated Tip cases; suction side squealer and full squealer blade tip geometries were manufactured as a solution for TLV. Both cases were observed in a linear turbine cascade which included seven High Pressure Turbine (HPT) blades and measurements were taken by means of Kiel

probe and Five Hole Probe (FHP). Measurements were taken with traversing the probes above 50% span and at one axial chord downstream to the blades. When velocity fields and total pressure measurements were gathered and examined in detail, it was seen that a complex vortex system consisting of TLV and passage vortex (PV) existed in the observed area. In addition, when squealer geometries were applied, TLV preserved its location but pressure loss was reduced and PV became very small and migrated through TLV. Also, there was one more vortex observed which was periodic; some interrogation and predictions about its identity were also made about it. All reported consequences of tip geometries were evaluated in both cases, and test results showed that full squealer performs better for reducing the pressure loss under the circumstances. Calculations made by the means of blade-passage averaged total pressure loss coefficient indicated that, with respect to the flat tip geometry, full squealer and partial squealer tip geometry reduced the pressure loss about 19% and 3%, respectively. And, for comparing and demonstration of the repeatability of the tests, FHP and Kiel probe total pressure loss distributions were cross-checked.

Keywords: Tip Leakage Vortex, Passage Vortex, cascade, flat tip, squealer tip geometry, Kiel probe, five hole probe

ÖZ

KANAT UÇ GEOMETRİLERİNİN AKIŞ VE KAYIP KARAKTERİSTİKLERİNE ETKİLERİNİN LİNEER TÜRBİN KASKAD DÜZENİNDE DENEYSEL İNCELENMESİ

ALİCAN, Ozan

Yüksek Lisans, Havacılık ve Uzay Bölümü

Tez Yöneticisi: Doç. Dr. Oğuz UZOL

Ocak 2017, 108 sayfa

Gaz türbinlerinde verim kayıplarına sebep olan bazı faktörler vardır. Bu turbomakinalardaki iç akışlar göz önüne alındığında, akış içerisinde oluşan girdaplar da bu sebeplerden bir tanesidir. Bu çalışmada gaz türbinlerinde uç girdabı olgusundan kaynaklanan verim kayıplarının oluşum mekanizması araştırılması amaçlanmıştır. Ek olarak, bu mekanizmalara göre, türbin kanatçıklarına iki uç geometrisi uygulanmış ve performans artışları gözlenmiştir. Bu çalışma, bir uç geometrisi en iyileme araştırmasının deneysel bölümüdür ve değişik uç geometrileri arasında HAD tabanlı araştırmalar ile en iyi performan olduğu raporlanan geometrinin test edilerek karşılaştırılmasını sağlayacaktır. Bu araştırma kapsamında, deneyler iki kolda sürdürülmüştür; düz ve uç geometrili kanatçıklar. Bu kollar “İşlem Görmemiş” ve “İşlenmiş” olarak isimlendirilmiştir. İşlem görmemiş durum, referans olarak kabul edilmiştir ve işlenmiş durumlara ait sonuçlar ise referans durum ile karşılaştırılmıştır. İşlenmiş durumlarda pasif bir akış kontrol yöntemi olan tam ve kısmi squealer geometrileri kanatçıklara uygulanmıştır. Bütün deneyler, 7 adet Yüksek Basınç Türbini kanatçığı bulunan lineer kaskad düzeneğinde Kiel ve Beş Delikli sensörler ile yürütülmüştür. Sensörler, kanatçık sırasının 1 aksel veter gerisinde ve kanat açıklığının üst %50 kısmında taşınarak ölçümler alınmıştır. Hız alanları ve basınç dağılımları detaylı olarak incelendiğinde, uç girdabı ve geçit

girdabından oluşan karmaşık bir girdap sistemi ile karşılaşmıştır. Uç geometrileri uygulandığında ise, uç girdabının etki bölgesi yeri korunmakla beraber genel basınç kaybının azaldığı, geçit girdabının ise oldukça küçüldüğü ve uç girdabına doğru hareketlendiği gözlemlenmiştir. Ek olarak, periyodikliği gayet iyi olan bir yapı daha gözlenmiş, kimliği konusunda bazı araştırmalar ve tahminler yapılmıştır. Elde edilen ölçümlerin tüm sonuçları değerlendirilmiş ve tam squealer geometrisinin basınç kaybı azaltma performansı açısından bu şartlar altında en başarılı geometri olduğu gözlemlenmiştir. Geçit ortalamalı toplam basınç kayıp katsayısı ile yapılan hesaplamalı karşılaştırmalarda, düz uçlu kanatçığa göre, tam squealer uç geometrisi ile %19 ve kısmi squealer uç geometrisi ile de %3 civarında iyileşme gözlenmiştir. Ek olarak, ölçümlerin karşılaştırılması ve tekrarlanabilirliğinin ispatlanması için Kiel ve Beş Delikli sensör ölçümleri karşılıklı kıyaslanmıştır.

Anahtar Kelimeler: Uç girdabı, geçit girdabı, kaskad, düz kanatçık ucu, squealer uç geometrisi, Kiel sensörü, beş delikli sensör

“Ben; ölen babamdan ileri, doğan çocuğumdan geriyim.”

- Kendinize, Bize ve bana dair hayalleriniz için...

Umulur ki gerçekleştirebilsin.

ACKNOWLEDGEMENTS

First and foremost, I wish to express my deepest and sincere gratitude to my supervisor Assoc. Prof. Dr. Oğuz Uzol for finding me worthy to be his pupil, for his endless support, patience, and knowledge.

I would like to thank all my thesis committee members; Assoc. Prof. Dr. Sinan Eyi, Assoc. Prof. Dr. M. Metin Yavuz, Asst. Prof. Dr. Harika S. Kahveci, and Asst. Prof. Dr. Sıtkı Uslu for reviewing my thesis and giving very valuable advices.

I wish to thank all members of expAero Team; Hooman Amiri, Yashar Ostovan, M. Tuğrul Akpolat, Anas Abdülrahim and Sinem Uluocak for tirelessly answering my never-ending questions and for their much appreciated friendships. This would not have been possible without them. I wish to thank my colleagues; Çağrı Gezgüç, Mert Erk and Mustafa Bilgiç who are good, real friends and never hesitated to help in my time of need and share my burden. Also, Nisa Şimşek and Utku Mutluer were very friendly and helpful to me through this journey.

I would like to express my sincere gratitude to Hakan İşçi, Murat Ceyhan and Taylan Ercan on behalf of TAI and TEI for supporting this thesis and their invaluable suggestions and Ali Oğuz Yüksel, Cansu Karataş, Gökçe Özgül, Mehmet Ali Yavuz, Ali Kıvanç Ersan and Senem Aktaş for their friendships. This study was funded by TAI under DKTM-2015-13 code.

I am truly thankful to my entire family, who raised me to become who I am today. My deepest thanks go to my father Ali, a true braveheart, my mother Fatma, a free spirit, and my brother Erkin.

I cannot express my thanks enough to my best friends who have been through it all with me. I cannot give all their names however much I may wish to, but I love them all the same. Many special thanks to my dear friends Gökhan Akdemir, Samet Dönmez, Ersay Gökbudak, İsmail Örtlek, Ayşen-Onur Aslan, Yasin Çetin, Mehmet Gökdemir, Hasan Hüseyin Kazan, Mustafa Ç and Dereboylu.

Since we were talking by percentages in this work, my $\geq 50\%$, my dearly beloved wife, Tuna ınkılılı Alican was, is and will be everything.

TABLE OF CONTENTS

ABSTRACT	v
ÖZ	vii
ACKNOWLEDGEMENTS	x
TABLE OF CONTENTS	xii
LIST OF FIGURES.....	xiv
LIST OF TABLES	xvi
LIST OF SYMBOLS	xvii
CHAPTERS	
1. INTRODUCTION.....	1
1.1 Flow Physics	3
1.1.1 Secondary Flow Structures and Flow Mechanisms.....	3
1.1.2 Entropy Generation Mechanisms	7
1.1.3 Classification of Loss	12
1.1.4 Estimated Losses Related to Tip Leakage Vortex.....	14
1.1.5 Theoretical Aspects of Loss Production of Tip Leakage Vortex	15
1.2 Possible Remedies for Tip Leakage Vortex	18
1.2.2 Active Flow Control Methods (Active FCMs).....	18
1.2.3 Passive Flow Control Methods (Passive FCMs)	21
1.3 Literature Survey on Squealer Tip Geometry	26
1.4 Aim of the Study	28
2. EXPERIMENTAL SETUP AND MEASUREMENT DETAILS	29
2.1 Wind Tunnel.....	29
2.2 Test Cascade Section.....	31
2.3 Blade Type And Tip Treatments	33
2.3.1 Flat Tip Blade / No Treatment Case.....	35
2.3.2 Squealer Tip Blade / Treated Tip Case 1.....	36
2.3.3 Full Squealer Tip Blade / Treated Tip Case 2	37

2.4	Wind Tunnel Characterization	38
2.5	Measurement Techniques, Data Acquisition And Post-Processing	43
2.5.1	Basic Information About The Experiments	43
2.5.2	Pressure Measurements (Kiel Probe)	45
2.5.3	Pressure / Velocity Measurements (Pitot-Static Tube)	46
2.5.4	Pressure / Velocity Measurements (5 Hole Probe)	47
2.5.5	Velocity Measurements (Hot-Wire Anemometry).....	50
2.5.6	Post-Processing	52
2.5.7	Measurement Uncertainties.....	52
3.	RESULTS AND DISCUSSION	55
3.1	Data Analysis	55
3.1.1	Total Pressure Analysis with Kiel Probe	55
3.1.2	Total and Static Pressure Analysis with Five-Hole Probe	56
3.1.3	Quantitative Evaluation of Measurement Results	58
3.2	Periodicity	60
3.3	Measurement Planning and Scenarios	62
3.4	Downstream Measurements with Kiel Probe.....	63
3.4.1	Low Resolution Measurements.....	64
3.4.2	High Resolution Measurements	67
3.5	Downstream Measurements with Five-Hole Probe	71
3.5.1	High Resolution Measurements	71
4.	CONCLUSION	91
	REFERENCES.....	95
	APPENDICES	
	A. DATA PROCESSING OF FHP.....	101
	B. UNCERTAINTY CALCULATIONS	104
	C. FHP DATA PROCESSING PROCEDURE	108

LIST OF FIGURES

FIGURES

Figure 1. 1: Flowfield near the the hub wall [2].....	4
Figure 1. 2: Flowfield near the casing wall [13]	5
Figure 1. 3: Mechanism of Tip Leakage Vortex [4].....	6
Figure 1. 4: Dissipation coefficient in different boundary layer regimes [4]	9
Figure 1. 5: h-s graph of turbine [4]	16
Figure 1. 6: A representation of jet blowers [20]	19
Figure 1. 7: A representation of plasma actuators [21]	20
Figure 1. 8: A representation of vortex generators [12]	21
Figure 1. 9: A representation of different squealer geometries	22
Figure 1. 10: A representation of winglets	23
Figure 1. 11: A representation of knife edges	24
Figure 1. 12: A representation of tip injection based on Auxier's patent [28]	25
Figure 2. 1: Sketch of the wind tunnel at METU Aerospace Dept. Lab	30
Figure 2. 2: A sketch of test section	33
Figure 2. 3: HPT blade profile.....	34
Figure 2. 4: A cross-sectional sketch of HPT bladewith flat tip and manufactured one	35
Figure 2. 5: A cross-sectional sketch of HPT bladewith partial squealer tip and manufactured one	37
Figure 2. 6: A cross-sectional sketch of HPT bladewith full squealer tip and manufactured one	38
Figure 2. 7: Location of inlet plane and inlet measurement lines (tunnel flow is through the plane of paper).....	39
Figure 2. 8: Calibration curves for low-resolution (left) and high-resolution (right) measurements	40
Figure 2. 9: Velocity (top), P_{tot} (mid) and turbulence intensity (bottom) graphs at the cascade inlet for low resolution measurements	41
Figure 2. 10: Velocity (top), P_{tot} (bottom) graphs at the cascade inlet for high resolution measurements	42
Figure 2. 11: A drawing of test section (top cover removed), measurement surface and projection of the test blade passage	44
Figure 2. 12: Kiel probe	46
Figure 2. 13: Pitot-static tube	46
Figure 2. 14: Five Hole Probe (FHP)[32].....	47
Figure 2. 15: Calibration setup of FHP at METU Aerospace Engineering Dept. Lab	49
Figure 2. 16: Carpet plot of FHP calibration map	50

Figure 2. 17: Hot wire calibration setup	51
Figure 2. 18: Coordinate system of probe, measurement plane and positioning of FHP (and Kiel probe)	52
Figure 3. 1: Formulas of velocity components (left), positive directions of FHP and orientation on observation surface	57
Figure 3. 2: The calculation window of $C_{p,m}$ on the measurement plane.....	59
Figure 3. 3: A sketch of test section (top cover removed) and positions of tailboards	61
Figure 3. 4: P_{tot} measurements at 50% span (top) and 65% span (bottom)	62
Figure 3. 5: P_{tot} distributions for flat tip (top), partial squealer tip blade (a) and full squealer (b) with Kiel probe in low resolution.....	65
Figure 3. 6: C_p distributions for flat tip blade (top), partial squealer tip blade (a) and full squealer (b) with Kiel probe in high resolution	68
Figure 3. 7: $P_{tot}/P_{tot,inlet}$ graph along 16,5% horizontal position.....	70
Figure 3. 8: C_p distribution for flat tip (top), partial squealer (a) and full squealer (b) with FHP measurements in high resolution	72
Figure 3. 9: C_p distributions for flat tip blade (top), partial squealer tip blade (a) and full squealer (b) with Kiel probe in high resolution	73
Figure 3. 10: C_p measurement (in grayscale) of Nho[36]	75
Figure 3. 11: P_{tot} and velocity vectors for flat tip (top), partial squealer tip (a) and full squealer (b) cases	76
Figure 3. 12: Vorticity and velocity vectors for flat tip (top), partial squealer (a) and full squealer (b).....	78
Figure 3. 13: P_{tot} and streamlines for flat tip (top), partial squealer (a) and full squealer (b)	79
Figure 3. 14: P_{st} and velocity vectors for flat tip (top), partial squealer (a) and full squealer (b).....	80
Figure 3. 15: 3 velocity component vectors for flat tip (top), partial squealer (a) and full squealer (b) (out-of-plane component (w) given with contour plot).....	81
Figure 3. 16: Q distributions along pitchwise direction at different span levels.....	83
Figure 3. 17: Streamwise velocity component (w) distributions along pitchwise direction at different span levels	84
Figure 3. 18: u and v velocity component distributions along 80% and 85% span levels	85
Figure 3. 19: u and v velocity component distributions along 95% and 97,5% span levels ..	86
Figure 3. 20: P_{tot} distributions along pitchwise direction at different span levels	87
Figure 3. 21: Vorticity magnitude along the 95% span level.....	89

LIST OF TABLES

TABLES

Table 2. 1: Wind tunnel specifications	31
Table 2. 2: Specifications of HPT blade profile	34
Table 2. 3: Specifications of flat tip geometry	36
Table 2. 4: Specifications of squealer tip geometry	37
Table 2. 5: Specifications of full squealer tip geometry	38
Table 2. 6: A summary of test conditions.....	43
Table 2. 7: Parameters of FHP measurements for calibration.....	48
Table 3. 1: $C_{p,m}$ calculation window coordinates on observation surface.....	58
Table 3. 2: Required parameters for $C_{p,m}$ calculations.....	59
Table 3. 3: Results of Kiel and FHP measurements and improvement percentages	90
Table B. 1: An example of FHP calibration data	104
Table B. 2: Average and absolute error values of FHP coefficients	105
Table B. 3: An example of data acquired from measurements	106
Table B. 4: Average and absolute error values of FHP coefficients	106
Table B. 5: Uncertainties of total / static pressures and velocity measurement	106

LIST OF SYMBOLS

<i>AC</i>	<i>Alternating Current</i>
<i>C_p</i>	<i>Specific heat under constant pressures (kJ/kg.K)</i>
<i>C_p</i>	<i>Total pressure coefficient</i>
<i>C_{p,m}</i>	<i>Blade passage averaged total pressure loss coefficient</i>
<i>C_{p,pitch}</i>	<i>Pitch angle calibration coefficient</i>
<i>C_{p,st}</i>	<i>Static pressure calibration coefficient</i>
<i>C_{p,tot}</i>	<i>Total pressure calibration coefficient</i>
<i>C_{p,yaw}</i>	<i>Yaw angle calibration coefficient</i>
<i>CV</i>	<i>Corner Vortex</i>
<i>FCM</i>	<i>Flow Control Methods</i>
<i>FHP</i>	<i>Five-Hole probe</i>
<i>h</i>	<i>Specific Enthalpy (kJ/kg)</i>
<i>HPT</i>	<i>High pressure turbine</i>
<i>HV</i>	<i>Horseshoe Vortex</i>
<i>LE</i>	<i>Leading Edge</i>
<i>Ma</i>	<i>Mach Number</i>
<i>P</i>	<i>Pressure (Pa)</i>
<i>PS</i>	<i>Pressure Side</i>
<i>PV</i>	<i>Passage Vortex</i>

<i>Re</i>	<i>Reynolds Number</i>
<i>RI</i>	<i>Rotating Instabilities</i>
<i>s</i>	<i>Specific Entropy (kJ/kg)</i>
<i>SS</i>	<i>Suction Side</i>
<i>T</i>	<i>Temperature (Celsius)</i>
<i>TE</i>	<i>Trailing Edge</i>
<i>TI</i>	<i>Turbulence Intensity</i>
<i>TLV</i>	<i>Tip Leakage Vortex</i>
<i>U</i>	<i>Freestream velocity at the inlet</i>
<i>V</i>	<i>Velocity (m/s)</i>
η	<i>Efficiency</i>
μ_{eff}	<i>Effective friction coefficient</i>

SUBSCRIPTS

<i>0</i>	<i>Total amount of thermodynamic entity</i>
<i>1</i>	<i>Inlet station</i>
<i>2</i>	<i>Exit station</i>
<i>is</i>	<i>Isentropic process</i>
<i>mean, m</i>	<i>Average value of the quantity</i>
<i>ref</i>	<i>Reference value of the thermodynamic entity</i>
<i>s,e</i>	<i>Static value of thermodynamic entity at the exit</i>

<i>st</i>	<i>static</i>
<i>t,e</i>	<i>Total value of thermodynamic entity at the exit</i>
<i>t,i</i>	<i>Total value of thermodynamic entity at the inlet</i>
<i>tot</i>	<i>total</i>
θ	<i>Momentum thickness</i>

CHAPTER 1

INTRODUCTION

In turbomachines, there is a tip clearance between the rotating blade tip and the casing wall in order to prevent the rubbing. The height of the gap is narrowing down with the latest improvements in production technologies. Nevertheless, it is impossible to totally eliminate this gap. And, since there is a pressure difference between the pressure and the suction sides of the blade arising from the nature of the main flow, this creates a flow through the tip clearance which can be considered as a leakage which is not desired. The leakage flow when combined with the mainstream creates a secondary flow phenomenon occurring in a turbomachine and it is called Tip Leakage Vortex (TLV).

These secondary flows should not be confused with the other sub-flows which are taking place within the turbomachine and having the purpose of cooling down the blades or bleed air taken from the main flow for other demands. In secondary flows, a small part of flow is diverted from main flow under the different effects (pressure difference between the sides of blade, leading edge stagnation point or boundary layer) and it cannot be directed enough to extract or impart work from or to it. In addition, due to other effects such as secondary flows, boundary layer or separation, it creates further penalty on efficiency. As in our case, in a turbine, a cancellation or weakening in the secondary flows creates better results in overall working conditions for the turbine and also for the entire turbomachine.[1]

These phenomena are highly encountered and investigated in large detail because they are important contributors to efficiency reduction in turbomachines in many ways. In recent years, investigations about the secondary flow around the rotor blades and blade passage increased in a very large number because the vortices around the blades and in the passage produce a large portion of efficiency drop. Sharma and Butler [2] predicted that 30% - 50% of the aerodynamic loss in axial turbine stator row are originated from the secondary flow at the endwall region. Besides, this increases the fuel consumption which is an important criterion in the field of aviation.

The efficiency drops which are created by TLV are produced by effective blockage of the blade passage[3], [4], strong mixing[5], [6] and producing noise and vibration[7]. Another mechanism is that TLV increases heat transfer from the main flow to rotor blade[8] which is a decisive factor on lifespan of blades. Also TLV may cause stall in compressors[9] which limits the stable operation range. In hydraulic turbomachines, TLV core is the base for cavitation.[10], [11]

In dealing with tip leakage flow, different solutions have been suggested. Those fall into two groups as Passive and Active Flow Control Methods (FCMs). Passive ways are easy to implement, no additional energy input is required but their effects are permanent through all the working conditions. Squealer tips, winglets and labyrinth seals/knife edges can be given as examples to passive methods and they are mostly based on geometric design solutions. Active schemes require energy input and application is a bit complex but they can be turned off when not needed. Jet blowers, plasma actuators and vortex generator jets are examples of these. These require some instrumentation and control systems.

The objective of this study is to investigate the main mechanisms behind the efficiency losses in gas turbine blades occurring due to Tip Leakage Vortex (TLV);

- using experimental methods
- in a linear cascade arrangement
- using a high pressure turbine rotor blade profile.

In this research, the results regarding the control of the TLV in blades treated with flat tip and squealer tip geometry and the influences of tip geometries on flow and loss characteristics will be reported.

1.1 Flow Physics

In this section, the physical sources of blade passage vortices, the ways of entropy generation and loss classification due to TLV will be explained. Then, entropy and efficiency of the turbomachine will be connected theoretically. And, precautions against TLV-based problems will be examined. Physical results and some past studies about TLV will be summarized.

1.1.1 Secondary Flow Structures and Flow Mechanisms

In secondary flow investigations, the vortex structures mainly encountered are namely;

- Passage vortex (PV)
- Horseshoe vortex (HV)
- Corner vortex (CV)
- Tip leakage vortex (TLV)

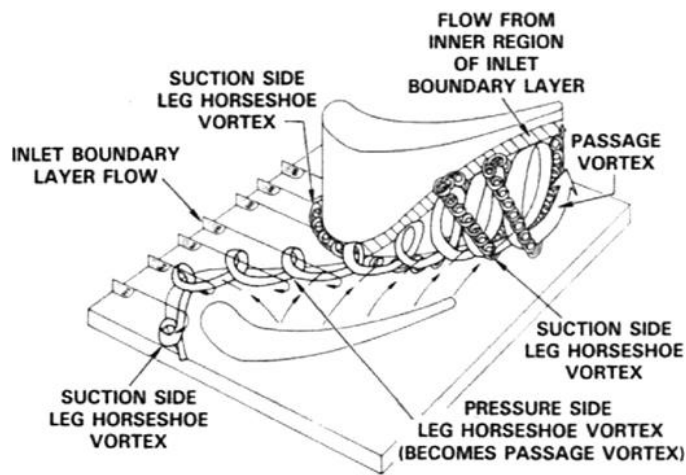


Figure 1. 1: Flowfield near the the hub wall [2]

These structures are continuously interacting with each other through the blade passage, especially PV, HV and TLV are foremost dominant vortex types and these are creating an important proportion of the efficiency losses. The HV originates from the endwall where boundary layer hits the leading edge of the rotor blade root. After the HV is created at the stagnation point, it separates into two branches and goes around the pressure and suction sides of the blade. While suction side HV is attached to the blade, pressure side HV then moves through the tip and the suction side of the successive blade and merges with the suction side branch of the HV to create the PV. [Fig. 1.1] Also local effects have important role in the creation of PV, examples of which are blade surface boundary layer and passage pressure gradients. These secondary flow structures are highly three-dimensional due to velocity gradients and high viscosity effect by the boundary layer. The PV creates a boundary layer separation at the suction surface of the blade and contributes to efficiency reduction via decreasing the production of lift. This can be very dangerous in low aspect ratio blades since it can cover most of the blade surface.[10], [12]

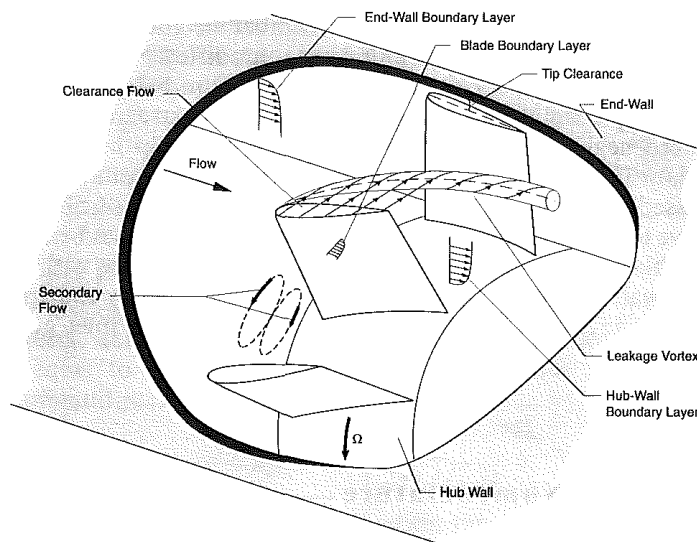


Figure 1. 2: Flowfield near the casing wall [13]

The TLV is created by pressure difference between the suction and pressure sides of the blade and flow takes place through the tip gap from pressure side to suction side. [Fig. 1.2] Flow enters from the corner of pressure side and creates a separation bubble at the tip surface. This separation bubble forms a vena-contracta. [14] After exiting from the suction side, flow increases its velocity and creates a jet, moves through the passage without detaching from the casing for a distance, and then it starts a vortex motion in streamwise direction. [Fig. 1.3] This turning to radial direction occurs because tip leakage flow jet clashes with the main flow and boundary layer separates. While growing, TLV migrates through the passage and keeps gathering the vortex filaments. At the eye of the vortex, TLV never unites as a point; rather it produces a coil of intertwined filaments. The TLV produces a total pressure loss at the exit of the blade passage and therefore significant efficiency reduction. Since the flow in the passage is highly complex, TLV and PV interact

closely, their adverse effects are similar and they enhance and affect each other.[10], [15]

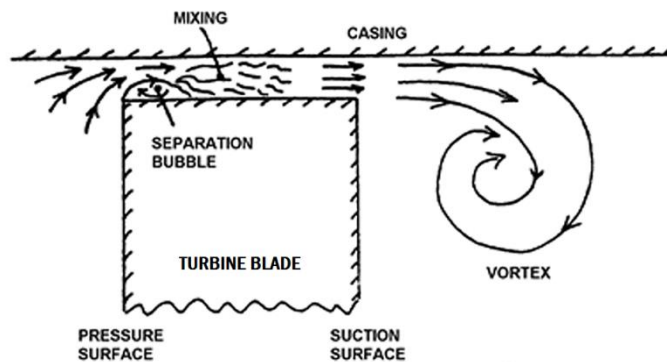


Figure 1. 3: Mechanism of Tip Leakage Vortex [4]

Since there is no way of removing the pressure difference between the suction and pressure sides of the rotor blade and the tip gap, TLV always takes place in a blade passage. Turbulence within the TLV is highly anisotropic (properties have directional independence) and non-homogeneous (positional independence) and it can be observed by tracing the high turbulent kinetic energy and high turbulent shear stresses. [10]

The mechanism of TLV can be summarized as;

- It starts to root up at the suction side of the tip.

- The eye of the vortex moves through the passage and pressure side of the next blade with creating the “shear layer” behind. Shear layer supplies vorticity to TLV at initial stages.
- At early phases of rollup, some vortices join into TLV.
- While moving through the blade passage, TLV loses connection with shear layer.
- Then some other vortices (like CV) wrap around TLV while moving through the passage.

1.1.2 Entropy Generation Mechanisms

Efficiency can be identified via enthalpy but this entity is not so proper for rotating turbomachines since relative stagnation enthalpy changes with radial location. Then, it comes to define the efficiency via entropy. Because unlike total enthalpy; entropy values do not change whether it is viewed from rotating or stationary blades and with the radius of the blade. The entropy increase can be calculated for each blade row and the results can be generalized to whole turbomachine. If we know another thermodynamic property of the fluid flowing at the exit, state of the fluid can be calculated at that row or stage. Then the total turbomachine efficiency is obtained.

Denton [4] outlined that the entropy generation occurs according to some fluid dynamics cases. These are;

1. Viscous effects and friction in boundary layer or shear layers
2. Heat transfer across finite temperature differences
3. Non equilibrium processes, like rapid expansion in shockwaves

1.1.2.1 Entropy Generation due to Viscous Effects and Friction

In tip clearance flow, blade surface boundary layers, shear layers (e.g. shear jet associated with tip leakage flow) and blade tip velocities play an important role; therefore, the effects of boundary layer and shear layer based entropy issues cannot be ruled out. In the following two subsections, these topics will be covered.

Entropy Generation In Boundary Layers: In the past studies, it is shown that primary entropy sources are where the velocity gradient is the largest, like boundary layers or shear layers. In the boundary layer scope, it is concentrated at the innermost sections of the region, in viscous sub-layer.

In the studies, entropy generation is handled as a dimensionless “dissipation coefficient” for being practical in calculations. These formulas are rather correlations of experimental data and give general results.[4] The formulas and the change with respect to Re based on momentum thickness are summed in Figure 1.4.

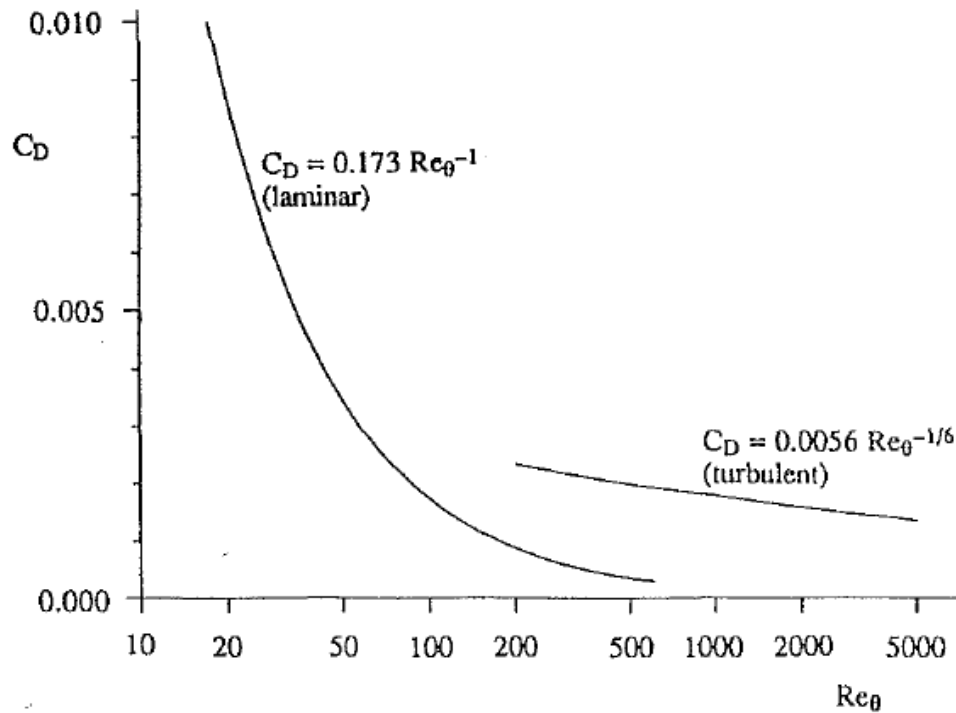


Figure 1. 4: Dissipation coefficient in different boundary layer regimes [4]

From the Figure 1.4, it can be seen that while the dissipation coefficient is sensitive to Re_θ in laminar boundary layer, in turbulent regime dissipation coefficient is relatively independent from it. This means, entropy generation which is analogously represented with dissipation coefficient, is closely related with boundary layer thickness. It is widely accepted [4] that in the turbulent boundary layer where $Re_\theta \geq 1000$, dissipation coefficient is around 0.002. Another important point is that in the range where laminar and turbulent boundary layer can both exist, $200 < Re < 500$, the dissipation coefficient changes considerably around 4 or 5 times. This also implies that the knowledge about the transition and the state of the boundary layer, whether it is laminar or turbulent, gains more importance.

About Mach number, there is no established result in existence. But the common range of Mach number in turbomachines is $0 < M < 2$ and the effect of it over the skin friction is very limited.

Entropy Generation due to Mixing: What mixing generally means is the existence of shear stresses and diffusion of temperature.[5] Entropy generation takes place where shear is the dominant factor. In the research of Li and Cumpsty, it is said that away from the endwall, the basic mechanism of mixing can be associated with the blade wakes and near the endwall, structures which are similar to blade wakes (separation, vortices, and leakage jets).[5] The mutual basic fact is; shear stresses are highly in effect in these turbulent sections. Since viscous dissipation is active in whole flow field, entropy generation is continuously active. But in the core region of the stream, this activity is relatively low with respect to the high shear regions. Since these structures are associated with turbulent flow and effective viscosity in these regions is larger than the laminar viscosity, local entropy generation rate in these regions is at important levels. But structures and flow interactions are so complex that quantification of entropy generation is rarely possible.

Separation will make larger vortices possible and an important ratio of entropy dissipation hence efficiency reduction source in the wake can exist.

Leakage jets undergo a mixing process in the tip gap and this is irreversible. So this creates entropy also.

In shear layers, if favorable pressure gradient is active on the streamwise direction the transverse velocity gradient, dV/dy , is reduced since slower fluid layers gain speed nearly more than faster layers. Therefore, shear strain and rate of entropy generation, which is proportional to $\mu_{\text{eff}} (dV/dy)^2$, will be reduced. This explanation shows us that acceleration of a shear layer and wake reduces dissipation and also mixing loss is reduced and deceleration increases.

1.1.2.2 Entropy Generation by Heat Transfer

It is obvious that heat loss always decreases work since the energy is loaded onto the flow by the means of heat. Hence, heat loss decreases work output. It should be minimized with insulation, if required.

The most important aspect of heat loss in turbomachines is the heat loss via cooling mechanism of turbine blades. After transferring heat to the cooling fluid, main flow produces less work than the adiabatically expanded case and cooling fluid produces more work. (Turbomachines are assumed to be well insulated.) But since main flow is larger in mass proportion, total work will be reduced.

In addition, the coolant will be subsequently introduced to main flow and it can cause other losses by disturbing boundary layer stability and state of boundary layer on blade surface and endwall.

In turbines, turbine inlet temperature and stage temperatures are important parameters imposed by designed thermodynamic cycle and work requirements; therefore, heat loss must be stopped. But at the other hand, after a certain point, turbine blades must be cooled down and held at that level continuously. In this subject, there is a sweet point which must be found in order to maximize the produced work.

1.1.2.3 Entropy Generation in Shock Waves

Shockwaves are inescapably irreversible; hence, they are clear sources of entropy. Entropy creation is due to high viscous normal/shear stresses and heat conduction within a molecular-order-thick shockwave.

The most serious event in turbines is the shock system which forms at the trailing edge of turbine blades. Entropy is generated by intense viscous dissipation at the edges of the separated region right after the trailing edge and the strong shock wave

bodies. Furthermore, shockwaves counteract with boundary layer also and in this situation, separation is likely and extra entropy generation is possible.

Turbines are generally designed to work under choked condition in most of the turbomachines; therefore, shockwave interaction with other flow structures is an important topic which must be handled with care. Oblique shocks may be preferred while designing turbine blades, since they produce less entropy than a normal shock with the same upstream Mach number.

1.1.3 Classification of Loss

Denton [4] outlined the loss breakdown in turbines, as the classical approximation, as follows;

- Profile Loss
- Endwall (Secondary) Loss
- Tip Leakage Loss

These are types of losses and nowadays it is understood that these cannot be taken as independent from each other. In the contrary, these are in close relation and in the following bullets, they are tried to be covered for turbine case.

Profile losses: These are related to the boundary layer on the blades which are far from endwalls. At these sections, flow can be thought as two-dimensional and additional loss from trailing edge also belongs to that part.

In order to minimize the boundary layer loss, boundary layer should be laminar as long as possible over the surfaces. In turbines, conditions such as Re , turbulence level and velocity distribution over the blade surface affect primarily and surface

roughness, transition point, solidity and inlet/outlet angles affect indirectly the behavior of boundary layer.

Trailing edge loss is underestimated especially for turbine blades because of neglecting the base pressure. The estimation or calculation of base pressure is not easy and attempts towards this aim was not productive. These efforts did not give correct correlations with measurements and yet they were able to give a general idea about the topic. In a research referenced by Denton (Mee, 1992), it is reported that one third of total loss is trailing edge loss due to mixing in subsonic conditions and this ratio rises nearly to fifty per cent in supersonic flow.

The effect of Mach number is that loss increases rapidly with approaching sonic conditions. In turbines, most of the loss increase related to Mach number is thought to be from trailing edge loss so the loss is because of mixing effect and base pressure. Then, one can conclude that trailing edge shape (thickness) affects the stage outlet plane shock system closely.

Endwall Loss: This is still referred as “secondary” loss because it is created and given shape by secondary flows (horseshoe vortex, passage vortex etc.) which arise on annulus walls of the blade passage. In an elementary meaning, it is the upstream boundary layer’s characteristics and total flow turning of the blade row that decides the strength and secondary flow features near the endwall, hence the intensity of endwall loss.

This is the most difficult element and all methods regarding this loss are still working with correlations without using any large physical explanation behind. Different researchers (Dunham, 1970; Dunham&Came, 1970; Sharma&Butler, 1987; Gregory-Smith, 1982) gave correlations to predict the endwall loss with using some different approaches which have little physics, yet some of these are widely used.

For turbines, endwall loss is a major source for losses which contributes nearly 1/3 of total loss.

Tip Leakage Loss: This is due to leakage flow over the tip of rotor blades and hub clearance of stator blades. The interaction between the tip leakage loss and endwall loss is very strong. At early times, this was thought as a similar concept to “Induced drag” as in the aircraft wing but it is handled as an inviscid effect since flow velocity at the tip gap is very high. (Re is high, so viscous effects are negligible) And in turbine blades, it is modeled as a two-dimensional orifice flow creating a total loss at the tip relative to no-clearance blade. Flow enters the tip gap from pressure side and separates from the blade tip and contracts to a jet. Until the jet contraction, as analogous to orifice throat, it is accepted as inviscid. And after the contraction, leakage jet mixes out in the tip gap and creates entropy by mixing effect. (Figure 1.3)

In turbines, it reduces the blade work and pressure drop for a fixed main mass flow rate, since this flow passes through the downstream without transferring its energy to blades. But since it is an inviscid atmosphere, it only creates a negative effect on mass flow-pressure ratio characteristic of the turbine rather than directly being an efficiency issue. And this mass flow change creates some lift loss on blades.

In addition, Yaras and Sjolander [16] reported that tip leakage flow recovers some of the energy by accumulating it on the tip leakage vortex as secondary kinetic energy. But at the downstream, recovered energy is definitely lost due to vortex mixes out with the main stream and vortex occurrence creates higher shear rates therefore entropy generation is faster. So, the energy is lost eventually, entropy generation is done and this accounts for the tip leakage.

1.1.4 Estimated Losses Related to Tip Leakage Vortex

There are some important factors and percentages need to be emphasized that affect the degree of efficiency reduction created by the TLV. The loss produced by tip gap is directly proportional to tip gap height and it can create a third of the total aerodynamic losses. [17] According to Lakshminarayana, [18] a tip gap of 1% of

blade span can create a reduction of 2-6% on turbine stage efficiency. Bindon [19] reported that 45% of the turbine rotor and a third of the turbine stage total aerodynamic losses can be created by TLV. In addition, an increase in the tip gap by 1% decreases the efficiency by 1,5% and increases the fuel consumption by nearly 3%. Also Bindon [19] reported that 48% of the total secondary flow-induced loss is produced by mixing of TLV with the main flow at the suction corner. Besides, 39% of the loss is produced in the tip gap and endwall losses due to shear and other secondary losses produce the remaining 13%.

1.1.5 Theoretical Aspects of Loss Production of Tip Leakage Vortex

While trying to give a theoretical explanation about how secondary flows generate the efficiency losses in a turbine stage, one must consider the entropy generation point of view.

To study that, entropy change in a turbine stage is considered. Under the assumption of thermally and calorically perfect gas, the entropy generation through a turbine is defined as

$$s - s_{ref} = c_p \ln\left(\frac{T}{T_{ref}}\right) - R \ln\left(\frac{P}{P_{ref}}\right)$$

We can assume the flow is adiabatic in a stationary linear cascade or rotating axial turbine. So the stagnation -or total- temperature change is negligible through the stage. Then entropy becomes the sole function of total pressure.

$$\Delta s = -R \ln \left(\frac{P_{t,e}}{P_{t,i}} \right)$$

Now, the debate comes to a new place of how entropy generation affects the efficiency. In a turbomachine, generally, isentropic efficiency is defined as the ratio of actual work to ideal (isentropic) work. In our case, it is defined as the ratio of actual work produced to ideal work. The factors which are violating the isentropic conditions have influence over the efficiency. The processes which are adiabatic and reversible are called as isentropic. So these reasons must be either heat transfer or thermodynamically irreversibility based disturbances. Since for most of the turbomachines flow can be treated as adiabatic, the only source remaining to produce entropy is irreversibility.

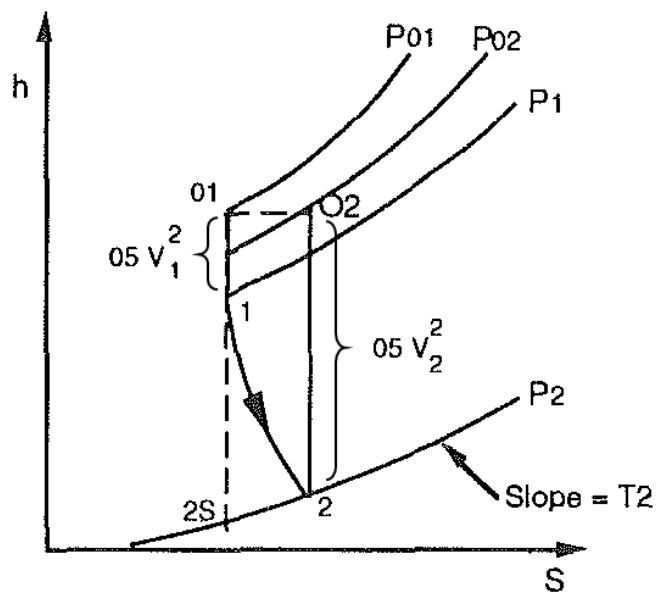


Figure 1. 5: h-s graph of turbine [4]

In Figure 1.5, the exit pressure line slope is assumed as local static temperature, T_2 , because of the fact that the slope of constant pressure lines on the h-s chart is equal to local static temperature. In other words, static temperature is constant along the P2 line. It is a reasonable assumption and is not seem to produce a significant error in our cases. [4]

Without taking into account the difference between static and total conditions and assuming no external heat transfer, the isentropic efficiency is given as

$$\eta_{tur,is} \approx \frac{h_1 - h_2}{h_1 - h_{2,is}} \approx \frac{h_1 - h_2}{(h_1 - h_2) + (h_2 - h_{2,is})}$$

$$\eta_{tur,is} \approx \frac{h_1 - h_2}{(h_1 - h_2) + T_2(s_2 - s_{2,is})} \quad (s_{2,is} = s_1)$$

If one puts the reference station to point 1 in Figure 1.5, sees that the isentropic efficiency is inversely proportional to the entropy generation. And since the entropy generation is shown with pressure changes, the pressure loss increases denominator and decreases the total value of the efficiency.

These equations show that, in order to improve efficiency in a stage -also in a whole turbine- we need to minimize pressure losses. Pressure losses are affecting the efficiency by entropy mechanism. Since these secondary flows create a huge effect by the means of pressure disturbances, their role on efficiency is clear. [4]

In the quest of investigations, total pressure loss can be tracked and recorded in a form of a pressure loss coefficient given as

$$c_{p,l} = \frac{P_{t,i} - P_{t,e}}{P_{t,e} - P_{s,e}}$$

With the help of this parameter, the performance of a turbine stage can be determined via measurable flow properties.

1.2 Possible Remedies for Tip Leakage Vortex

After the flow mechanics are understood to a large content, some solution methods and devices are proposed. These solution approaches are classified in two distinct groups as Active and Passive Flow Control Methods (FCMs).

1.2.2 Active Flow Control Methods (Active FCMs)

Active Flow Control Methods are more sophisticated and require and employ more smart equipment than passive ones. Because of these factors, installation is complex. In addition, these methods may require higher level production methods, drilling or casting holes in or through the blades. And since they need some energy input for its actuators, energy is taken from the work produced by turbine which is not desired. On the other hand, they can conduct their roles in a proactive manner by having some actuators, sensors and electronic feedback mechanism. These can be turned off completely or applied in sufficient levels according to flow requirements. The important point is, since there is nearly no change the exterior surface of the blade; they do not produce any additional adverse effects while turned off.

Jet Blowers: These jet blowers are a line of holes used for injecting coolants for blades at the hub endwall. [Fig. 1.6] If jets are going to be used, the jet holes and the flow rate are arranged with the purpose of weakening or suppressing HVs and PVs to produce additional benefit. Since these vortices are highly linked with TLV, jet

blowers has also impact on it. These holes are generally positioned in upstream of the connection point of blade LE and endwall. [20]

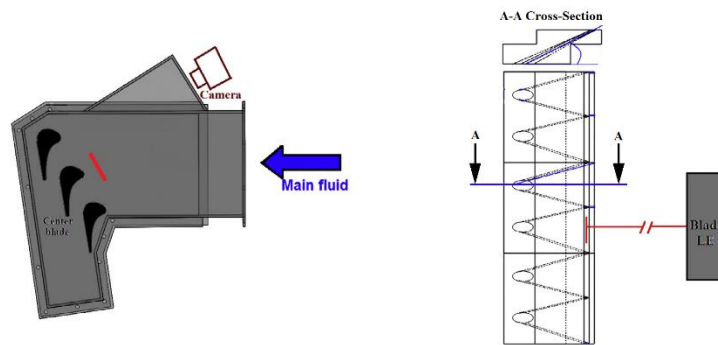


Figure 1. 6: A representation of jet blowers [20]

Plasma Actuators: Plasma actuators are a kind of active measures and it works by means of electric potential. System employs two electrodes in staggered configuration with a dielectric media between them. [Fig. 1.7] These electrodes are mounted in blade tips using with a dielectric matter. [1], [21]

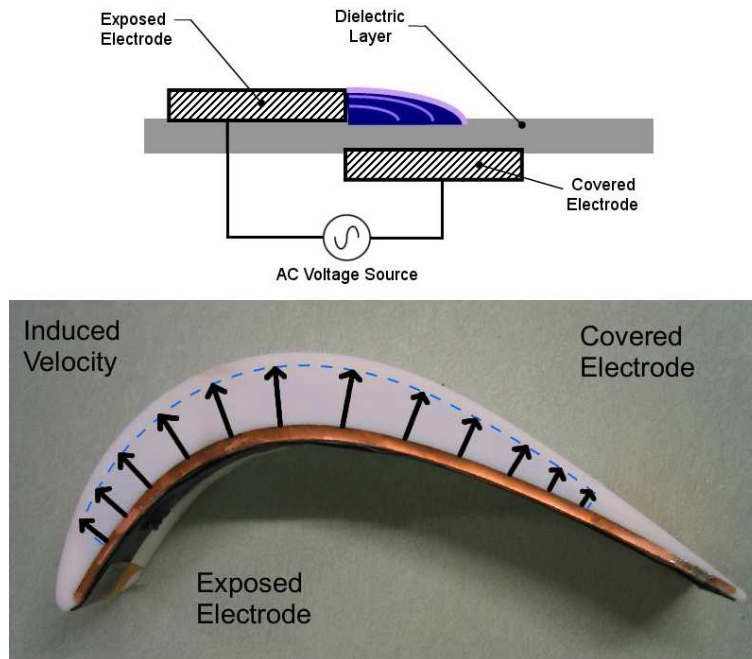


Figure 1. 7: A representation of plasma actuators [21]

With applying a certain level of AC voltage to electrodes, an electric potential is generated which ionizes the air in the tip clearance region. The ionized air moves under the presence of the electric potential and creates a body force which can be used to eliminate the adverse consequences of tip leakage flow.

Vortex Generator Jets: These vortex generators also aim to reduce the HV and PV-sourced losses hence the TLV. As separation occurs at the endwall, this method is strongly based on commanding this separation event. This measure either tries to induce the transition or reduces the separation probability by drawing the high momentum fluid into the near wall region. Separation is at least delayed in both ways by having turbulent flow and high momentum in boundary layer near wall region.[12]

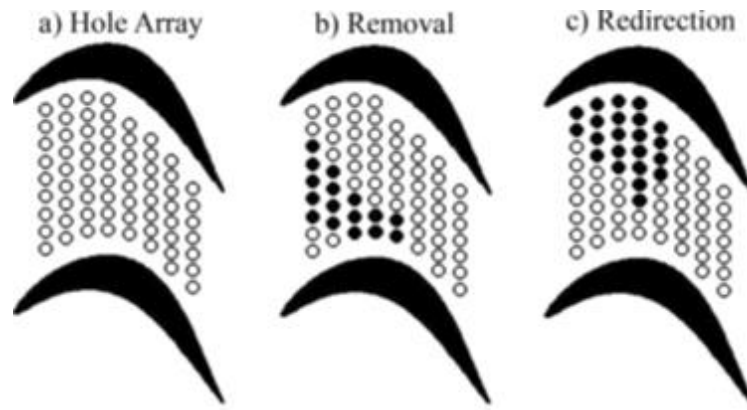


Figure 1. 8: A representation of vortex generators [12]

One typical arrangement consists of a set of holes located near the peak C_p of the turbine blade. Other is a number of holes installed on the blade passage endwall. [Fig. 1.8] In these formations, steady or unsteady blowing and suction is available. [12]

1.2.3 Passive Flow Control Methods (Passive FCMs)

Passive Flow Control Methods are mostly geometric applications at the tip of the blade. They are relatively simple, easy-to-apply and cost-friendly because they do not include any moving or electronic parts. There is no energy input and control instruments are not needed, which is an advantage. However, since they are fixed, these produce some adverse effects when not working at the design condition. This means, if you are working at off-design conditions, this has a significant adverse effect on efficiency issues in a gas turbine.

Since they are geometric modifications at the tip section as mentioned, they save the tip surface and corners from deformation in a remarkable amount. Instead of whole

tip surface, a section of blade tip stands against the casing wall and protects the tip from excessive deformation of heat and rubbing.

Squealer Blade Tips: A squealer tip is a blade tip geometry where a thin band of the blade tip is extended in spanwise direction and becomes closer to casing than any other point of the blade tip. There are two kinds of squealer tips exist, namely full (cavity) squealer and partial squealer. In full squealer type, the extended section forms a wall all around the blade having a “cavity” in the middle. And the partial squealer has a band either suction side or pressure side of the blade.[17]

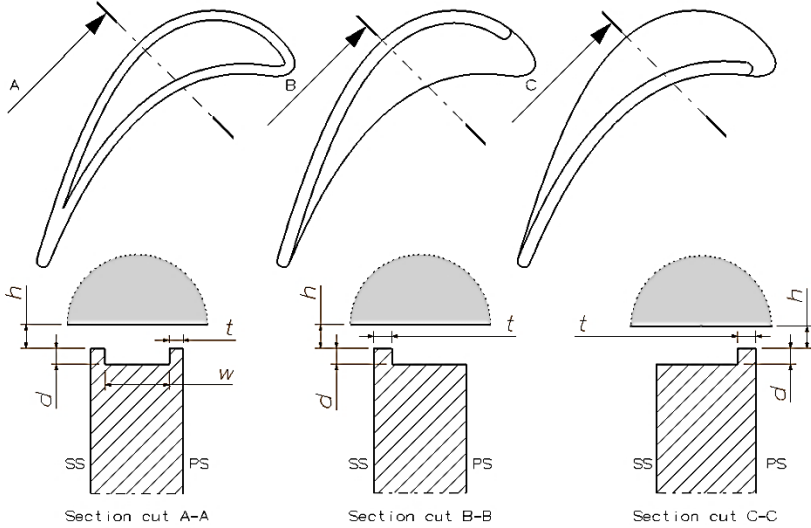


Figure 1. 9: A representation of different squealer geometries

Squealers may produce some drawbacks while turbine is not working at design point. But it helps by decreasing the mass flow rate of tip leakage flow in any situation and certainly makes TLV weaker by reducing the clearance.[22] Besides, squealer band section can be considered as a disposable section to save the whole blade tip and its geometry against the rubbing of blade and casing. Then, the squealer can be repaired during the maintenance actions. [23] And, since it has a certain curvature, it recovers and turns some of the leakage flow through the main flow and gains some of the work that is already lost. In addition, it produces a lower local heat transfer coefficient and protects the blade. [21]

Winglets: Winglets are geometric extensions which are at the same level with the tip surface. Winglets have no extension modifications through the tip clearance; they cover the suction or pressure side of the tip section instead. [Fig. 1.10] Also in some cases, both suction and pressure side winglets are offered.[24]

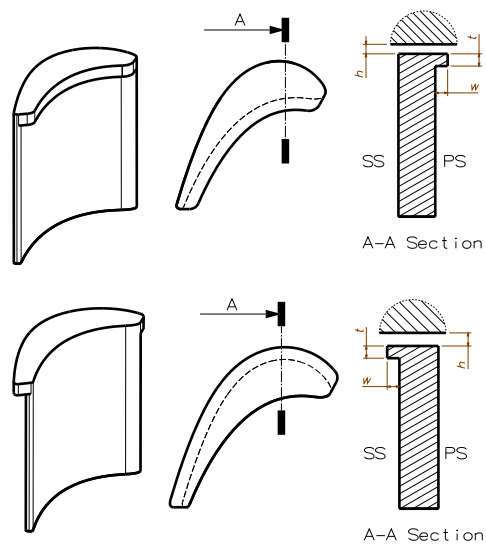


Figure 1. 10: A representation of winglets

It is thought that, the utilisation of winglets reduces the tip leakage flow by lowering the pressure difference between pressure and suction sides of the blade. Since this pressure difference is vital to the tip leakage flow, mass flow rate and loss at the clearance is effectively decreased. [24] Also Lee et al. [25] reported that, the pressure side winglets are inclined to reduce the adverse effects of TLV by producing resistance to tip leakage flow.

Labyrinth Seals and Knife Edges: These are again geometric variations for tip surface similar to squealers but a more primitive version. [Fig. 1.11] And, there is no turning for the tip leakage flow and these serve more to the purpose of locking the tip clearance for any flow. They are often employed as sets which include 2 or 3 of them. As predicted, these also try to cancel the pressure difference by simply standing.[26]

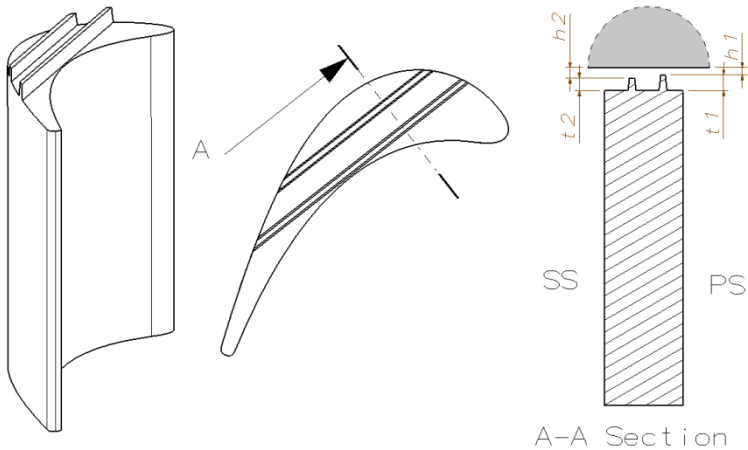


Figure 1. 11: A representation of knife edges

Tip Injection: In recent years, a new concept of Passive FCM came into picture. Spontaneous tip injection method falls into Passive FCM class because it occurs due to similar reasons with tip leakage flow. This injection flow is created by the pressure difference between the pressure side of the blade and the blade tip which the pressure difference between these locations is in the nature of the flow. This flow is directed with a hole from pressure side through the tip surface and aimed against the tip clearance flow to suppress it.[27]

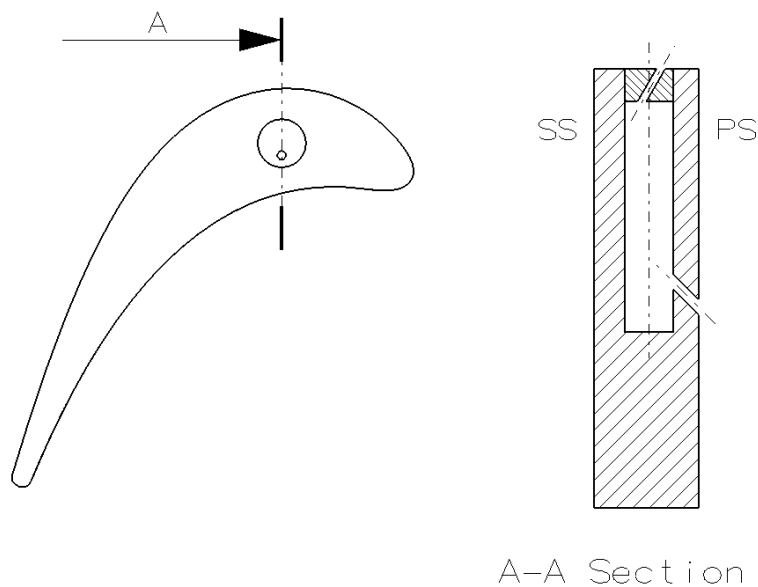


Figure 1. 12: A representation of tip injection based on Auxier's patent [28]

The first concept of tip injection [Fig. 1.12] is brought by Auxier [28] and applied for a patent in USA in 1995. Some others worked to improve this concept. But due to

confronted difficulties in measurements, conducted numerical studies could not be verified via experiments.

1.3 Literature Survey on Squealer Tip Geometry

Since the beginning of the secondary flow investigations, some significant mechanisms have been reported about which detrimental effects are produced by TLV and how they manifest on efficiency of turbomachines. Khalid, [3] presents and also reports from Smith and Cumpsty in his work that passage blockage can be thought as similar to “displacement thickness” in Boundary Layer Theory, it causes a reduction in blade passage area through which main passage flow goes (effective blade passage area) and this reduction is due to local velocity defects, for example axial or chordwise element of flow velocity decreases because of flow diversions. And this causes a pressure loss throughout the passage which in turn directly affects the efficiency. TLV also enhances mixing by producing highly turbulent sections. And then, TLV produces efficiency reductions due to mixing. Li & Cumpsty [4]–[6] and Denton reported that the blade wakes and unsteady motions in TLV create a high rate of shearing which is associated with turbulence and these intensify efficiency losses. Denton [4] also stated that mixing effect produces efficiency reduction by considerable amount of entropy generation. In addition, Mailach [7] presented that tip vortex produces detectable fluctuations and this is a basic reason of rotating instabilities (RI), which is the direct source of noise and vibration. And Tan [9] summarized that one of the possible origins of stall in the compressor is the tip leakage flows in the rotor blades. In this work, researchers conclude that, in a near-stability working conditions, a flow non-uniformity can create a local flow separation and hence a reduction in the effective blade passage area. That brings the compressor stalled and insufficient. In hydroturbomachines, TLV causes cavitation. Arndt [11] [11] presented in his work that cavitation is produced by the eye of the tip vortex, where local pressure gets lower. It also contributes to vibration and noise by

explosion of the bubbles at the high pressure regions and shortens the life of blades. Lastly, Azad, Han and Boyle [8] reported that TLV produces high heat transfer rate especially in an increasing trend with larger tip clearances which causes earlier physical deformation on blade tips. That is because a larger tip gap increases the mass flow rate of tip leakage flow, hence the heat transfer coefficient. And the tip geometry deviations from intended design creates further penalty on efficiency of the turbine.

In the previous works about the Passive FCMs, research topics generally concentrate on winglet and squealer tip treatments. These both produce promising results and give enough motives to further investigations.

However, researchers report some drawbacks about the winglet type tip treatments recently. Lee et al. [25] reported in his work in 2012 that, eventhough pressure side winglet application makes the TLV weaker, it has the tendency to fortify the subsequent passage vortex by supplying flow into it. In addition, pressure side winglet may initiate and promote the corner vortex just under itself which corner vortices have the lowest of chances to appear. And with respect to the flat tip case, winglets' improvement on the efficiency is proven to be smaller than cavity squealer tip.

On the other hand, the results given by Camci and Dey [17] about "Suction Side Partial Squealer Tip" configuration are highly positive. They show that partial squealer tip efficiently closes the tip gap which is an effective way to reduce the TLV. Dynamic total pressure measurements at the upper quarter of blade stage exit surface exhibit a noteworthy improvement in total-to-total efficiency. In the tip vortex dominant region, it is reported that total-to-total efficiency increases 5.01% and in a circumferential region efficiency increases 3.2%.

1.4 Aim of the Study

In previous investigations, many different flow control techniques belonging to either active or passive method class were devised and analysed via numerical and experimental ways. But in this thesis, a Passive FCM will be investigated. Because, in consideration of a turbine, this method is easy to apply in realisation, there are a large number of studies done before and it is reported to be most positive precaution against the TLV.

This study investigates the basic ideas and the mechanism behind the tip leakage flow and vortex attached to it. This objective will be achieved in a linear cascade arrangement with experimental methods using a HPT rotor blade profile. After a detailed review of literature, it is decided that one unique suction side squealer tip and one full cavity tip design will be employed on a HPT blade. An iterative and meticulous design phase for squealer geometries will be carried out to achieve a design which minimizes the negative effects of the passive methods. This design phase is done the numerical branch of this work and the resultant tip geometries are decided. After the experiments, the results of flat, squealer and cavity tips will be compared, the effects of squealer tips will be evaluated with respect to the flat tip and a summary will be presented. The experiments will be performed in a blow-down tunnel and five hole and Kiel probes will be used for velocity and pressure measurements.

This thesis is consisting of Chapter 2-Experimental Setup and Measurement Details, Chapter 3-Results and Discussion and Chapter 4-Conclusion sections. Experiment cascade, tunnel and measurement equipment will be presented in detail in here, Chapter 2. Data acquisition, processing and post-processing will be discussed also. In Chapter 3, measurement results will be given and detailed debate will be done. And in Chapter 4, findings will be summarized in an orderly fashion and further developments and investigations will be pointed out.

CHAPTER 2

EXPERIMENTAL SETUP AND MEASUREMENT DETAILS

In this section, the experimental setup and measurement operations will be presented in detail. First, wind tunnel and test section will be introduced. After that, information regarding the blade profiles and our reference and examining cases will be given in depth. Lastly, measurement equipment and data processing phases will be discussed.

2.1 Wind Tunnel

In this work, experiments will be conducted with a blower type tunnel which is located in the Aerospace Engineering Department Laboratory of METU. [Fig. 2.1] The basic dimensions are given in the figure below.

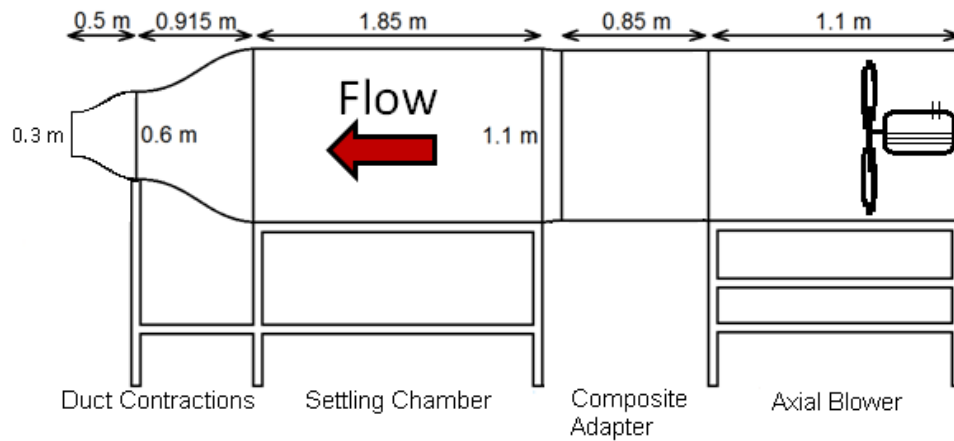


Figure 2. 1: Sketch of the wind tunnel at METU Aerospace Dept. Lab

The tunnel includes a single-intake axial type fan of 1,2 m. of diameter which is powered by a frequency-controlled 45kW AC electric motor, a 0,85m long composite adapter and a 0,915 m long duct with an area based contraction ratio of 3,36. After this section, another duct with the contraction ratio of 2 is employed for square to rectangle transition in order to connect with the cascade section. Composite adapter section transforms from the 1.2 m. diameter circular cross section to 1.1 m x 1.1 m. square section. Design details of the contraction and settling chamber sections of wind tunnel are presented by Ostovan [29]. Wind tunnel specifications are tabulated in Table 2.1.

Table 2. 1: Wind tunnel specifications

Wind Tunnel Specifications	
Motor Power (kW)	45
Fan Diameter (m)	1,2
Composite Adapter Length (m)	0,85
Settling Chamber Length (m)	1,85
First Contraction Duct Length (m)	0,915
First Contraction Area Ratio	3,36
Second Contraction Duct Length (m)	0,5
Second Contraction Area Ratio	2
Wind Tunnel Exit Area (m x m)	0,6x0,3

2.2 Test Cascade Section

In this study, a linear cascade section [Fig. 2.6] will be used to examine the tip leakage and related events. It can be said that the linear cascades are very different than rotating turbomachines hence it may not display phenomena sufficiently. But while working with rotating test sections, there are a number of difficulties encountered, such as blade and main shaft production, measurement problems, rotation, high Mach numbers and high freestream turbulence levels. These are very serious complications and in some cases, could not be coped with enough success ever since the investigations began. In addition, there are some sources in the literature concluding that linear cascades are performing more than sufficiently well under decent designs which are aiming to investigate special phenomena.

Jian Pu et. al. [20] noted that in order to provide a reasonably detailed and widespread insight about the secondary flows in blade passages, linear cascades have

repeatedly used in previous works. Its advantages are being simple in geometry and giving reliable and decent performance in measurements under the logical assumptions. Some precautions has been made such as, cascades having at least 3 passages are preferred to ensure periodicity. Also, El-Batsh [30] reported that linear cascades have a freedom of incidence angle change and simpler adjustment. Additionally, they are usually employed as a tool to supply quasi-three dimensional blade-to-blade data for the flow simulations. And, linear cascades make more detailed measurements in different regions of flow possible. When the experiment is ended, the reliability of the collected data from linear cascade is improved by using numerical calculations. The most important point is, results of the linear cascade can be used to decide which turbulence model is proper to that investigated case and numerical techniques can be validated. They concluded in the same study that linear cascade can be used instead of annular one because linear cascade produces reasonable results, experiment costs can be reduced and required mass flow rate is lowered in a considerable manner.

Our test section is produced on an aluminum profile structure. Base plate and side walls except one are aluminum and upper walls and one side wall are Plexiglas plates. The inlet and other dimensions are given in the drawing below.

Test section has the inlet cross section of 0.6 m x 0.3 m and designed to include 7 blades in a single row. In addition, it has a rotating circular table of 0.75m radius and stagger angle is variable since this table can rotate with blade row.. Blade pitch, p , is 110mm. At the inlet, there is a window where a turbulence grid can be attached if required. And, test section has a pair of bleed gates at the inlet and a pair of tailboards at the exit. [Fig. 2.2]

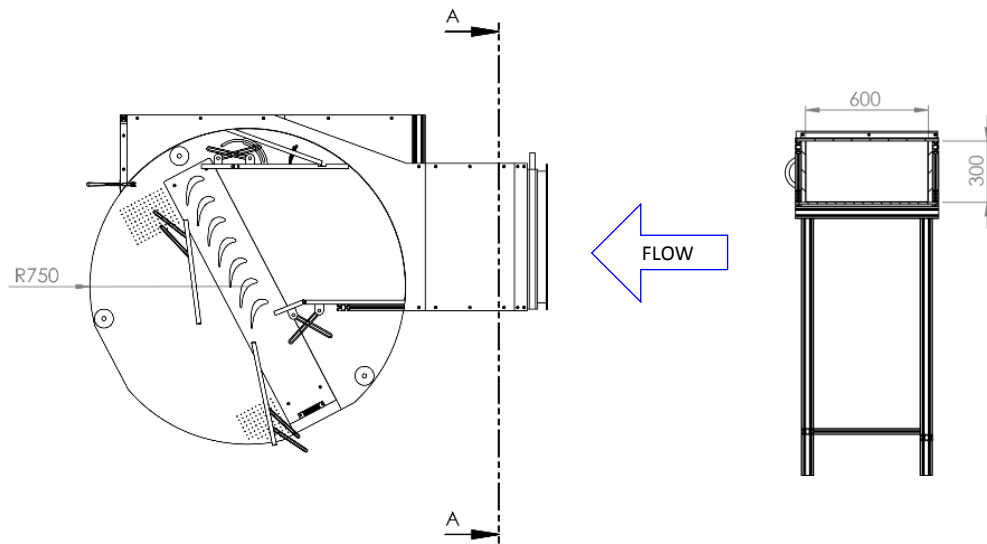


Figure 2. 2: A sketch of test section

2.3 Blade Type And Tip Treatments

In both –reference and investigated- cases; our blade profile will be the same. We will use a unique blade which is designed to use in the second stage of a high pressure turbine (HPT). The blade profile and detailed specifications of the blade are as given in Figure 2.3 and Table 2.2.

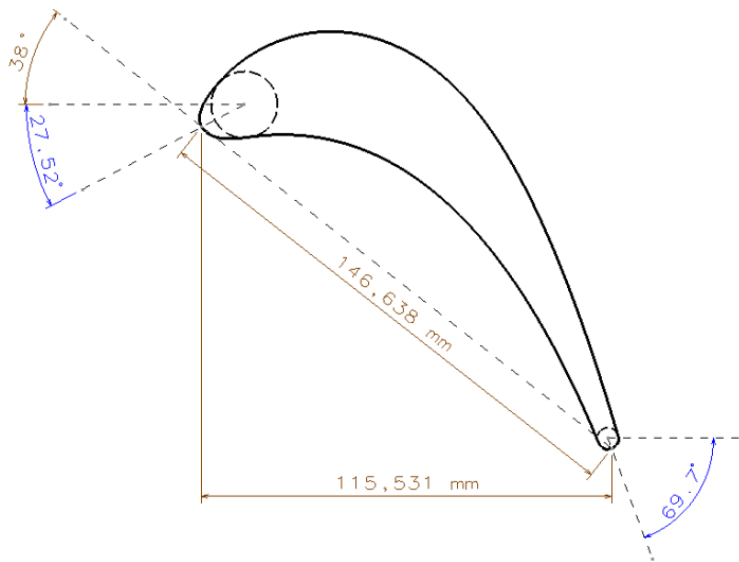


Figure 2. 3: HPT blade profile

Table 2. 2: Specifications of HPT blade profile

HPT Blade Profile Specifications	
Blade Profile	HPT 2.stage
Chord Length, c (mm)	146,6
Turning Angle	97
Stagger Angle	38
Flow Inlet Angle	27,52
Flow Outlet Angle	69,7
Pitch-to-Chord Ratio	0,75
Span, s (mm)	297
Tip Clearance, h (mm) / % of span	4 / 1,34

2.3.1 Flat Tip Blade / No Treatment Case

As mentioned before in the Chapter 1, the blade profile will be used without any measures taken against the tip leakage flow and the vortex associated to it. After the tests are carried out, results of this case will be collected by the means of pressure and velocity and used as a comparison with treated tip cases. A representative drawing, a photo of the blade and specifications of the blade is given in Figure 2.4 and Table 2.3.

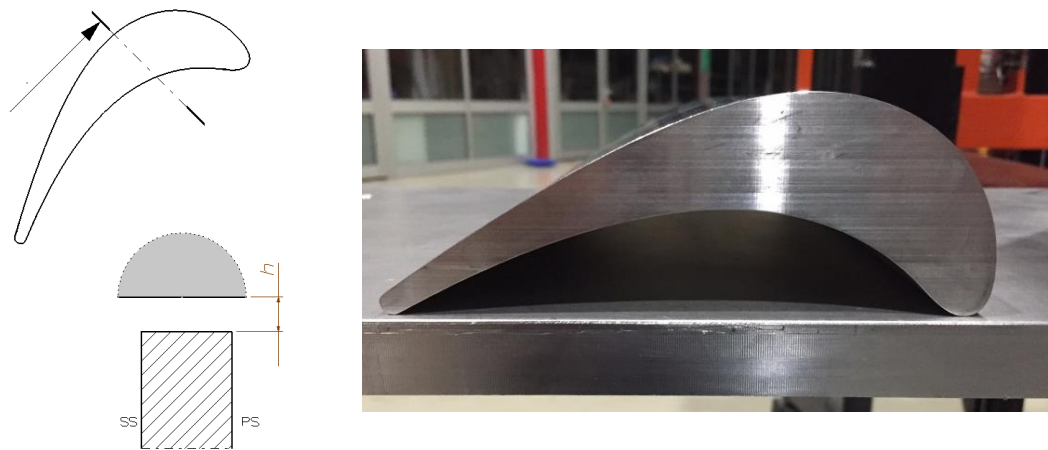


Figure 2. 4: A cross-sectional sketch of HPT bladewith flat tip and manufactured one

Table 2. 3: Specifications of flat tip geometry

Flat Tip Blade Specifications	
h (Tip clearance)	4 mm
d (Squealer depth from the tip)	0
t (Squealer thickness)	0

2.3.2 Squealer Tip Blade / Treated Tip Case 1

In this case, a unique squealer tip geometry will be applied to the same blade profile and results of the case will be compared to those of flat tip so that the performance of the squealer tip geometry can be clearly understood.

The design of the squealer geometry is carried out and the drawings and details of the squealer are given in Figure 2.5 and Table 2.4.



Figure 2. 5: A cross-sectional sketch of HPT bladewith partial squealer tip and manufactured one

Table 2. 4: Specifications of squealer tip geometry

Squealer Tip Blade Specifications	
h (Tip clearance)	4 mm
d (Squealer depth from the tip)	7,2 mm
t (Squealer thickness)	3 mm

2.3.3 Full Squealer Tip Blade / Treated Tip Case 2

In this case, a full cavity geometry is designed and applied to the same blade profile and results will be compared to the flat tip and also to the squealer tip and the most promising application will be decided. A picture of the full cavity blade and the specifications of the blade are given in Figure 2.6 and Table 2.5 below.

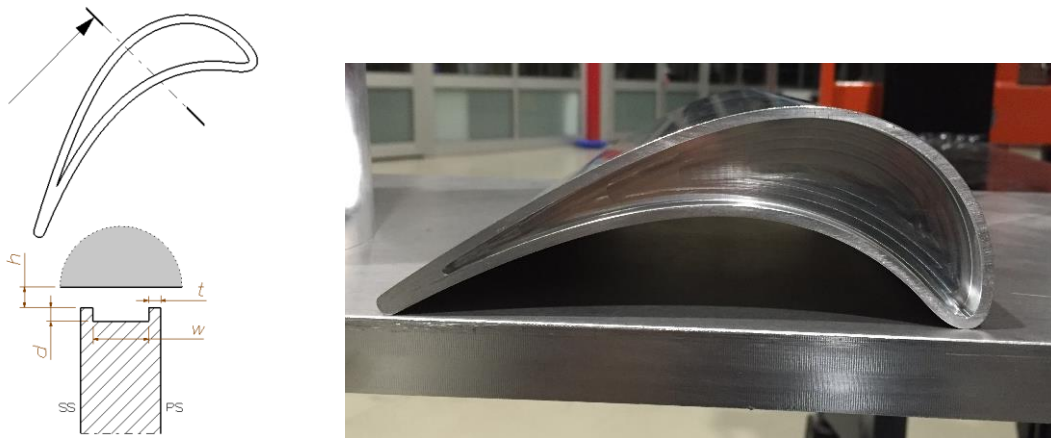


Figure 2. 6: A cross-sectional sketch of HPT blade with full squealer tip and manufactured one

Table 2. 5: Specifications of full squealer tip geometry

Full Squealer Tip Blade Specifications	
h (Tip clearance)	4 mm
d (Squealer depth from the tip)	7,2 mm
t (Squealer thickness)	3 mm

2.4 Wind Tunnel Characterization

At cascade inlet, in order to obtain the information about the velocity, total pressure levels and turbulence intensity, freestream is measured for different motor speeds and for each bleed gate configuration. Since motor is AC-type, motor speed is driven

with a frequency management device and measurements are done at the cascade inlet plane. Measurement directions are marked in a drawing of cascade inlet plane in Figure 2.7.

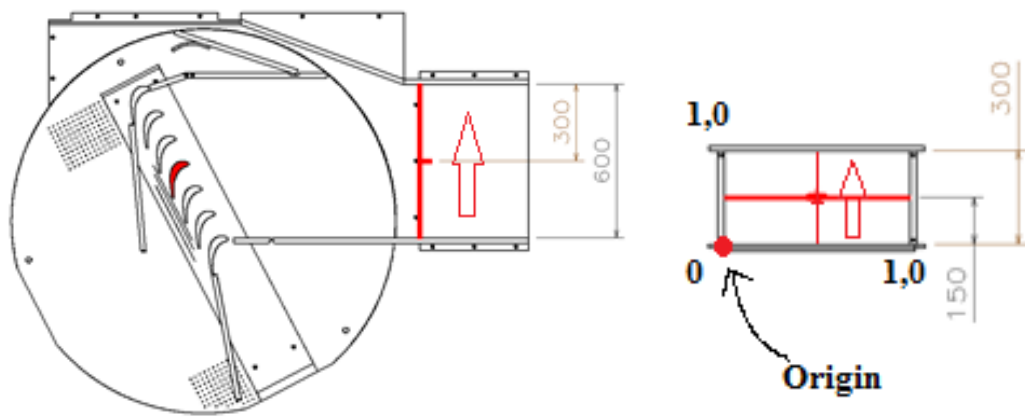


Figure 2. 7: Location of inlet plane and inlet measurement lines (tunnel flow is through the plane of paper)

Measurements are done with Kiel probe, pitot-static tube and hot wire, and calibration results are summarized in Figure 2.8.

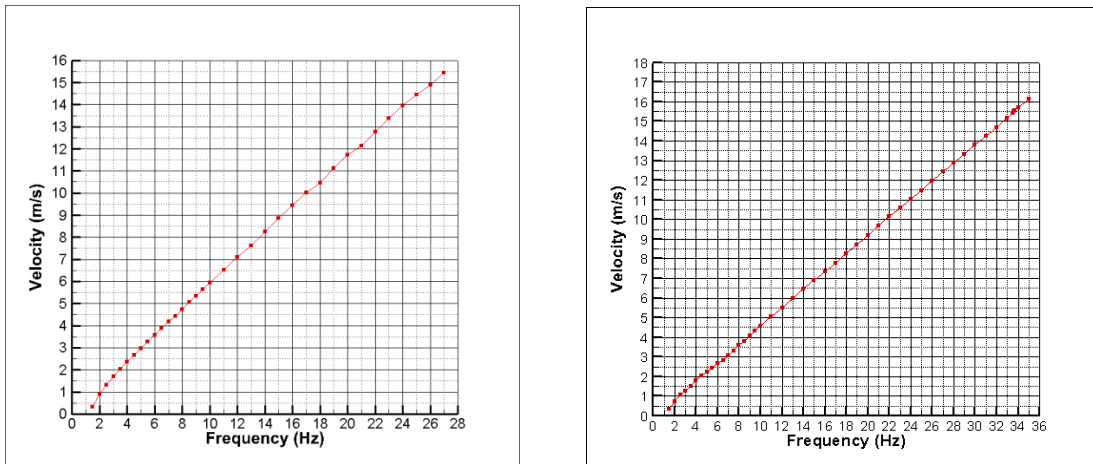


Figure 2. 8: Calibration curves for low-resolution (left) and high-resolution (right) measurements

Once calibration is done, motor is run with the adequate frequency to maintain the required velocity and measurements are made about axial velocity, turbulence intensity and total pressure using pitot-static tube and hot wire. All this calibration phase is done in the same conditions of those will be used in the experiments. [Fig. 2.9 and Fig. 2.10]

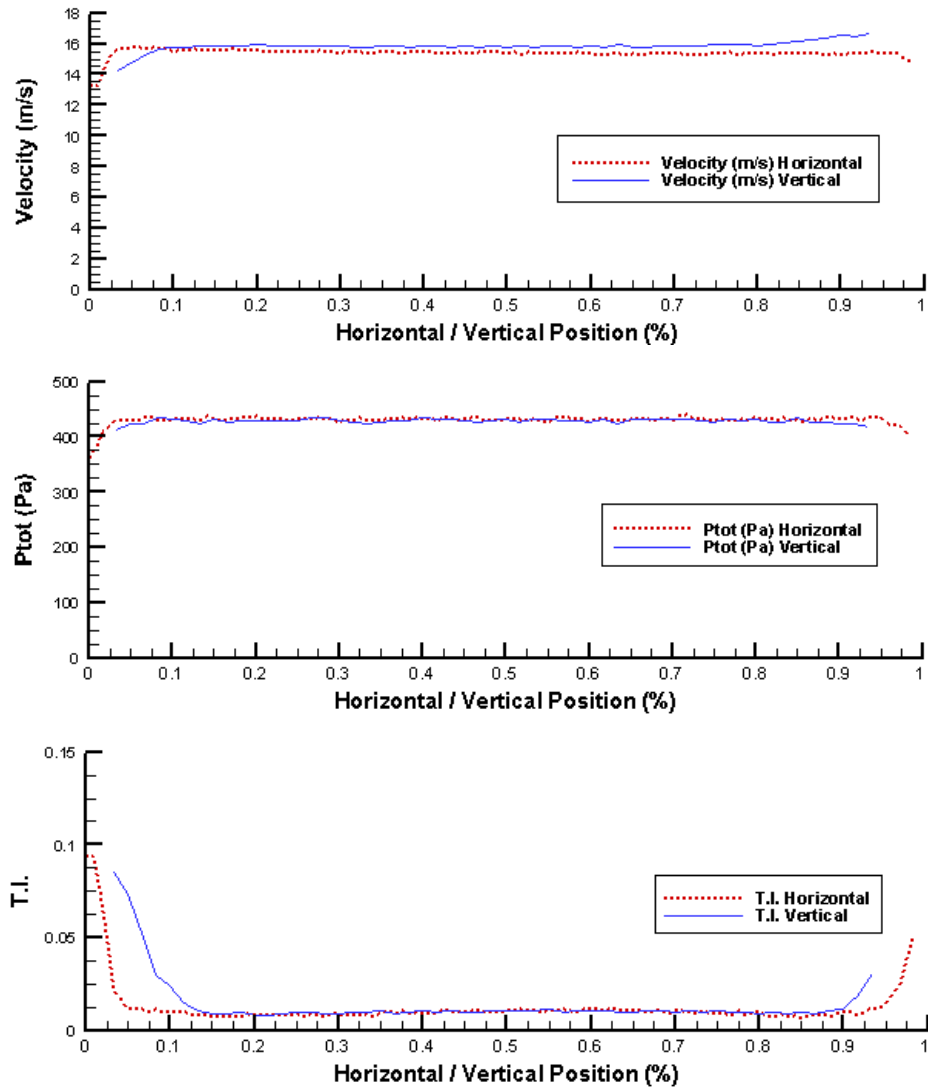


Figure 2. 9: Velocity (top), P_{tot} (mid) and turbulence intensity (bottom) graphs at the cascade inlet for low resolution measurements

The slight rise in horizontal velocity distribution in low resolution case is tried to be minimized. But it is the best distribution and since blade row is diagonal, outward velocity remains slightly faster (difference $\leq 0,2$ m/s) all the time. In addition, turbulence intensity at the inlet is below 1%.

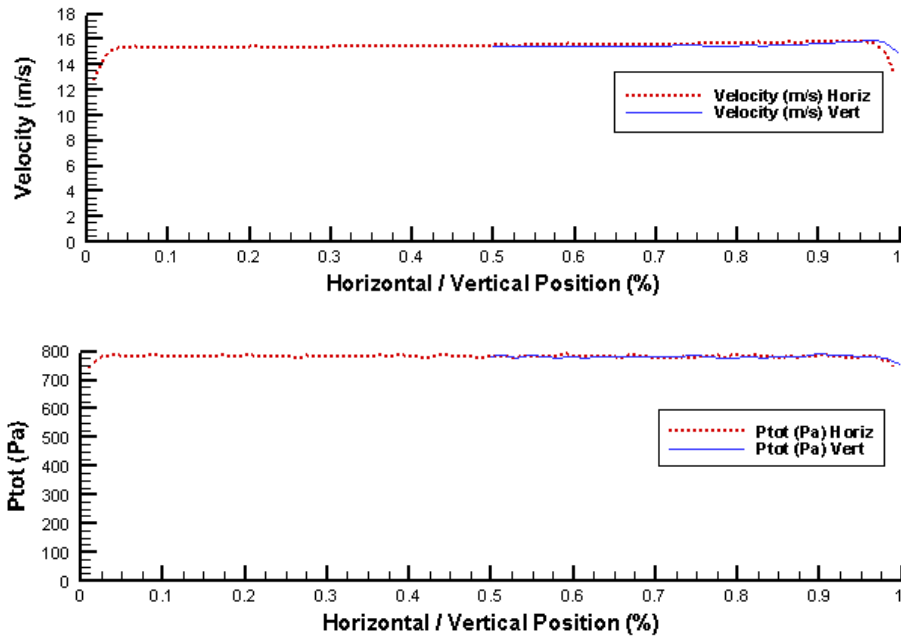


Figure 2. 10: Velocity (top), P_{tot} (bottom) graphs at the cascade inlet for high resolution measurements

In high resolution measurements, only the top half of the vertical direction is observed in order to understand the vertical velocity distribution whether gets effected from the possible air gaps or not. This makes that region suspected and some measures are taken in order to prevent air leakages. Also, this measurement clarifies and proves that this behavior is nature of the flow at inlet of the cascade and under the control in negligible effect levels. In addition, turbulence intensity levels are almost the same, so new inlet measurements are not added for high resolution case.

2.5 Measurement Techniques, Data Acquisition And Post-Processing

In here, measurement techniques which are going to be used in the experiments will be described in detail. The devices and the locations of the conducted measurements will be introduced and their specifications will be presented.

2.5.1 Basic Information About The Experiments

Table 2. 6: A summary of test conditions

Test Conditions			
	Low Resolution Case (Kiel Probe)	High Resolution Case (Kiel Probe)	High Resolution Case (5Hole Probe)
Velocity @ cascade inlet	15,5 m/s ($Ma \approx 0,045$)		
Re_{ch}	126000	132000	
Re Characteristic Length	Blade Chord (=146,638 mm.)		
Incidence Angle	0^0		
Mean Room Temperature	29^0 C	22^0 C	
Atmospheric Pressure	915 hPa	913 hPa	
Relative Humidity	75%	40%	
Flow Media	Air		
Dynamic Viscosity	$1,88 \cdot 10^{-5}$ kg/m*s	$1,84 \cdot 10^{-5}$ kg/m*s	
Kinematic Viscosity	$1,80 \cdot 10^{-5}$ m ² /s	$1,72 \cdot 10^{-5}$ m ² /s	
Density	1,042 kg/m ³	1,073 kg/m ³	

As given in Table 2.6, Reynolds number is based on the chord and the inlet velocity of the blades. Flow inlet and stagger angles are set as the values given in the Chapter 2.3 and incidence angle is set as 0° by rotating the bottom plate of the cascade.

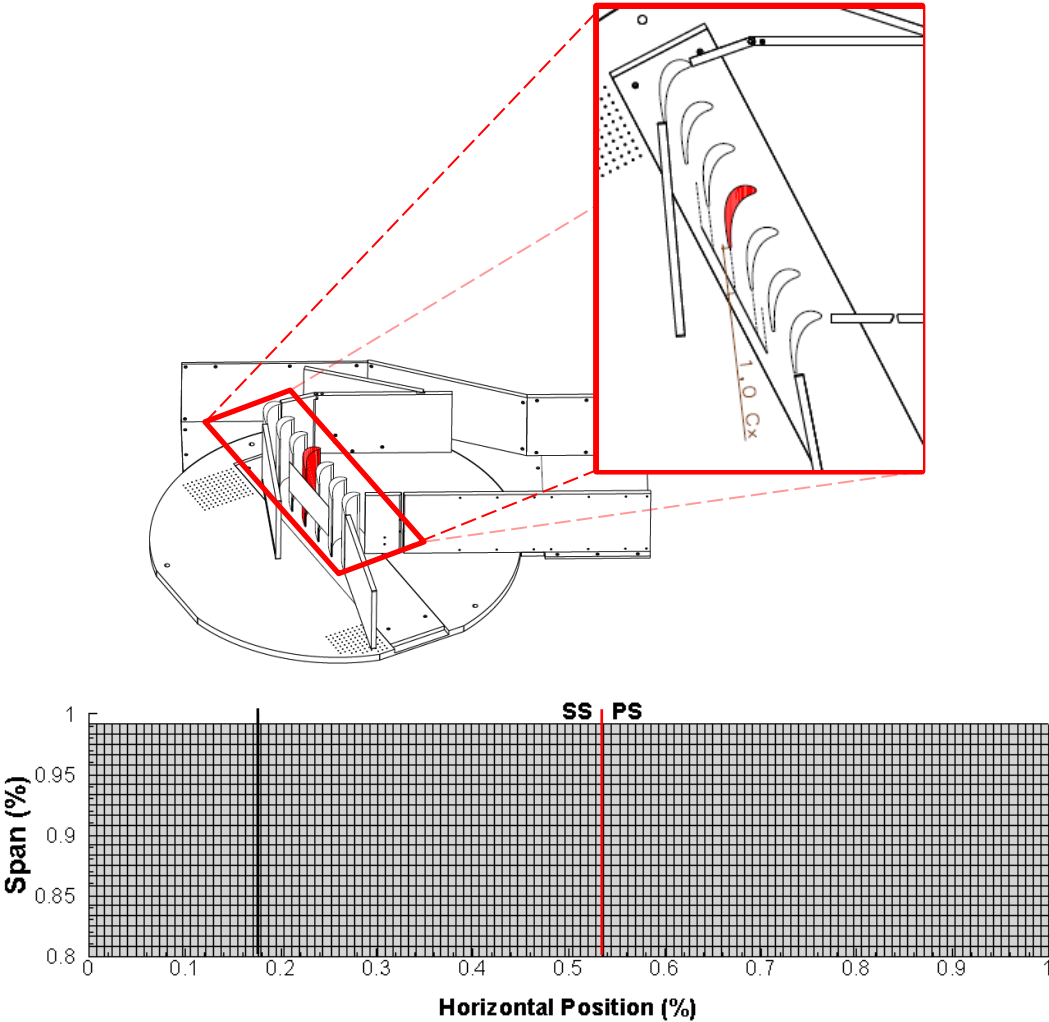


Figure 2. 11: A drawing of test section (top cover removed), measurement surface and projection of the test blade passage

All measurements at the downstream are made at 1 axial chord downstream of the blade row. In low resolution case, observation window covers from midspan (50%) to top casing (100%) and $\pm 1,5$ blade passage, making an area of 15 cm x 33 cm. This measurement section is scanned with 5mm resolution in horizontal and 15mm in vertical direction which produces 1980 points. In high resolution case, observation window covers from 80% of the span to top casing (100%) and resolution is 2,5mm in both directions which makes 3168 points. At each point, 300 samples are taken using the data-acquisition system. Traverses and the data acquisition system of all measurements are controlled via LabView. Measurement location is shown with black line in red rectangle and projection of test blade and neighboring blade are shown with red and black vertical lines on measurement plane respectively in Figure 2.11.

These experiments carried out with two different Re_{ch} at low and high resolution measurements. Weather conditions due to seasonal changes altered laboratory conditions and the difference in Re_{ch} is tried to be kept at minimum. Additionally, in the literature, it is seen that the difference of that amount did not create drastic changes in the nature of this type flow.[31]

2.5.2 Pressure Measurements (Kiel Probe)

Total pressure measurements are carried out using a United Sensors Kiel probe [Fig. 2.12] which has a 3,175mm shroud diameter and Scanivalve DSA3217 pressure transducer.

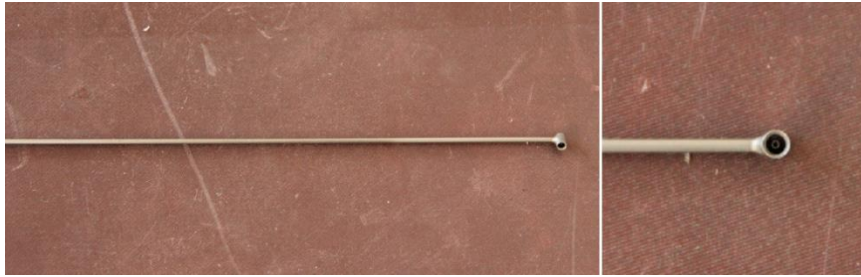


Figure 2. 12: Kiel probe

2.5.3 Pressure / Velocity Measurements (Pitot-Static Tube)

For total and static pressures and velocity measurements, pitot-static tube [Fig. 2.13] is used with Scanivalve DSA3217 pressure transducer. The diameter of the tube is 1,76mm.

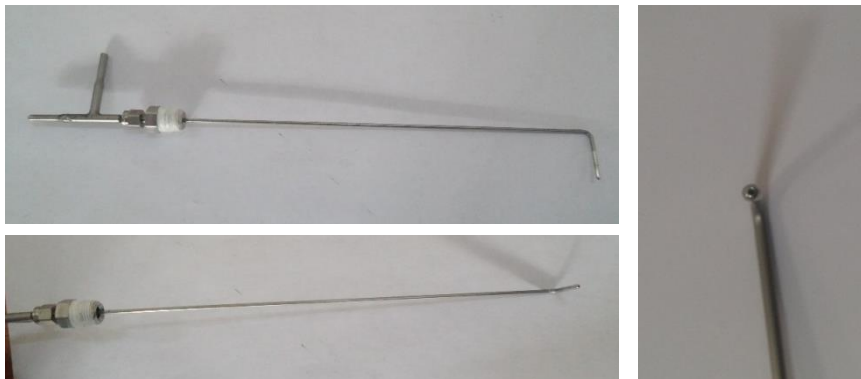


Figure 2. 13: Pitot-static tube

2.5.4 Pressure / Velocity Measurements (5 Hole Probe)

For total and static pressures and velocity, a five hole probe is also used. With this method, velocity field is obtained at the specified region with components. This gives the possibility of observing vortices in a more detailed manner and streamlines are made available. Again, Scanivalve DSA3217 pressure transducer is used for data acquisition. The diameter of the tube is 1,64mm. A representative figure and the five hole probe used in tests are given in Figure 2.14.

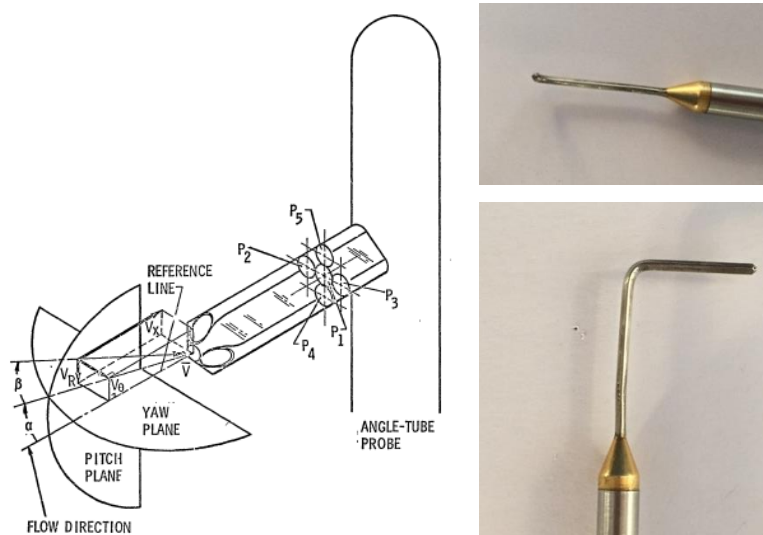


Figure 2. 14: Five Hole Probe (FHP)[32]

For using this probe, the mean velocity level at the observation window has to be determined approximately at first. For this aim, pitot-static tube is mounted to the test section and positioned in different regions of the specified observation region. But these points are selected to be as far away from the secondary flow effects as possible. The conditions of this measurement and the average velocity are tabulated in Table 2.7.

Table 2. 7: Parameters of FHP measurements for calibration

Temperature	20.4 ⁰ C
Atmospheric Pressure	905.8 hPa
Relative Humidity	22.1%
Dynamic Viscosity	1,84*10 ⁻⁵ kg/m*s
Kinematic Viscosity	1,71*10 ⁻⁵ m ² /s
Density	1,073 kg/m ³
Re _{ch} @ Inlet	132000
P _{tot,avg}	794,62 Pa
P _{st,avg}	37,62 Pa
U _{mean}	≈37,5 m/s

After this step, five hole probe has to be calibrated according to U_{mean} and calibration map (C_{p,pitch} vs. C_{p,yaw}) is going to be drawn and C_{p,tot} and C_{p,st} will be calculated for yaw and pitch combinations. For this, a new setup [Fig. 2.15] is constructed at the Aerospace Engineering Department Laboratory at METU. In this

setup, two VELMEX rotary traverses are used to move the five hole probe in angular step sizes and Dantec calibration jet is used to produce the appropriate level of velocity. A photo of the calibration setup is given in Figure 2.15.

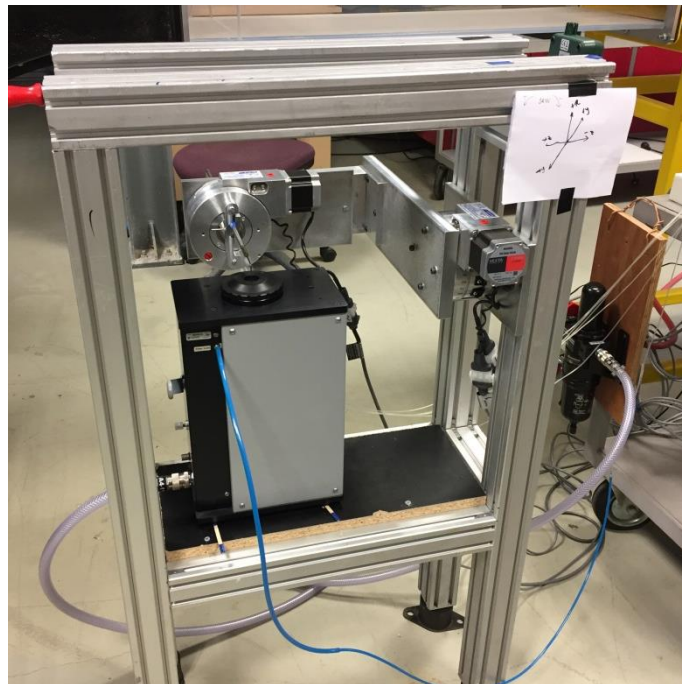


Figure 2. 15: Calibration setup of FHP at METU Aerospace Engineering Dept. Lab

In this setup, probe is moved by 1 degree step sizes between $\pm 27^\circ$ in yaw and pitch angles which is the expected angle interval in flow. A non-nulling calibration procedure is used based on Treaster and Yocum.[32] The calibration map is also obtained and given in Figure 2.16.

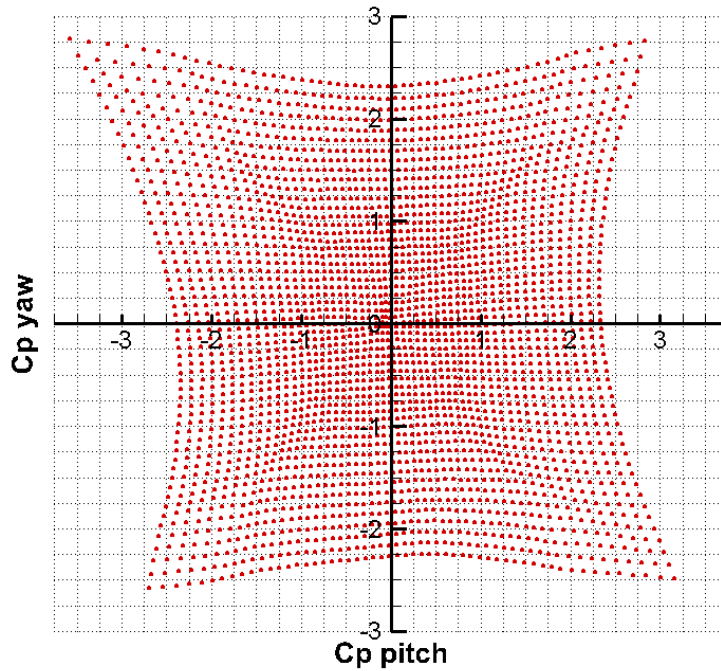


Figure 2. 16: Carpet plot of FHP calibration map

This calibration map is used to find the flow angles and resultant velocity values. For resultant velocity, total and static pressure values are used and velocity components are calculated from angles. Then, velocity distribution on the observation window can be found. Also total and static pressures will be available.

2.5.5 Velocity Measurements (Hot-Wire Anemometry)

For the velocity and turbulence information at the inlet, a CTA type Dantec 54N81 and NI9205 analog input modules are used to acquire data from single sensor hot wire probe. [Fig. 2.17]

Since this method is affected by temperature changes, hot wire sensor is calibrated before the measurements at each time. For calibration of the sensor, Dantec calibration jet is used.



Figure 2. 17: Hot wire calibration setup

As a final reminder for probes, the orientation of the FHP and Kiel with the measurement plane is given in Figure 2.18. In the figure, it is seen that probe is aligned with the streamwise direction. Hence, the streamlines and horizontal velocity components will be shown as their projections on the measurement plane.

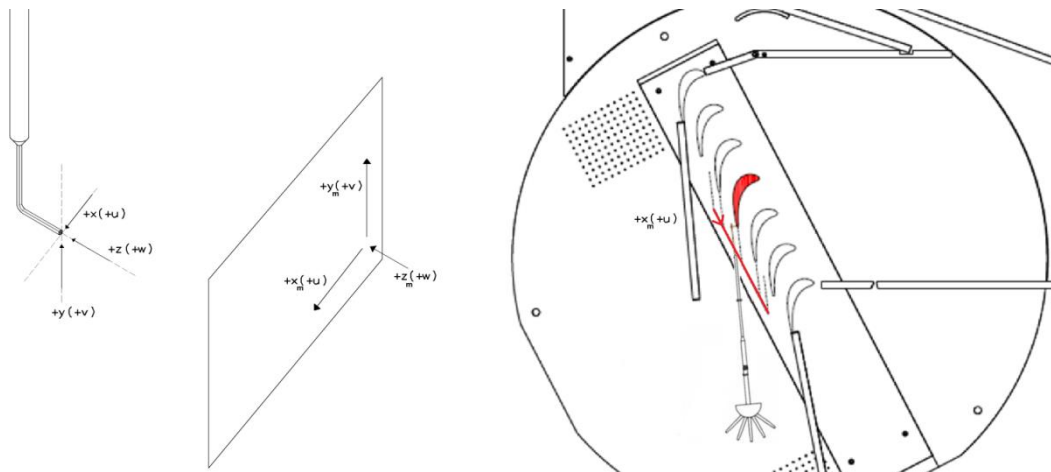


Figure 2. 18: Coordinate system of probe, measurement plane and positioning of FHP (and Kiel probe)

2.5.6 Post-Processing

For post-processing of the collected data, TecPlot is used to produce meaningful graphs. And a Matlab code is used in order to process the five hole probe data. This code is given in the Appendix 1.

2.5.7 Measurement Uncertainties

Physical Boundaries: This element is valid for Kiel and five hole probes. For five hole probe, it is reported in Treaster and Yocum [32] that there is a distance limitation for the probe from the walls. If probe is within these reported limits, results will be distorted. In measurements, a special attention is paid that the probe is outside of this limit. The same restriction is also valid for Kiel probe but since the

shape of the probe is more complex and robust than five hole probe (by the means of shroud and collecting the flow with it), Kiel probe is less affected.

Data Reading Variations: The variations in data acquisition phase is checked whether it has an important impact or not. In the FHP data, repeated measurements show that the variations are in within 2%. Since the same pressure transducer is used in all pressure measurements, this value is nearly valid for all probes. Inlet velocity values show a variation value of <0,5%. In addition, 300 samples are taken for all points in the measurement grid.

Reynolds Number: Re is slightly different for low and high resolution measurements. In the work of Matsunuma,[31] it is reported that there are very small changes occur in the flow characteristics and total pressure loss coefficients for that level of difference in Re. In addition, this Re difference creates nearly no change in tip leakage vortex loss.

Other Effects: In addition to these, there are some additional issues that produce uncertainties. For example, the slots which are used to put the probes in the flow and any other openings which may give harm to flow tried to be sealed as good as possible in order to prevent any undesired air leaks from test section. But eventhough, some of them may not be fully coped and some of the effects are unavoidable.

CHAPTER 3

RESULTS AND DISCUSSION

3.1 Data Analysis

3.1.1 Total Pressure Analysis with Kiel Probe

For total pressure measurements and in connection to this, for results; there are some coefficients defined in order to gain more insight and interpret in a clearer way. These are given as follows.

First, “total pressure loss coefficient” is defined as given below.

$$C_p = \frac{P_l - P_i}{\frac{1}{2} \rho U_i^2}$$

In this formula, P_l represents the measured total pressure which belongs to points of 1 axial chord downstream measurement plane which is defined at the Chapter 2. P_i is the upstream total pressure and U_i is the upstream freestream pressure.

Then, for more detailed and figurative comparisons, “blade passage averaged total pressure loss coefficient” is defined as;

$$C_{p,m} = \frac{\bar{P}_{tot,m} - P_i}{1/2 \rho U_i^2}$$

In this definition, $\bar{P}_{tot,m}$ represents the average of measured total pressures of test blade passage section at 1 axial chord downstream plane which will be defined in this chapter. This slight change produces a different figure than the other and gives an idea about the whole region of special importance.

3.1.2 Total and Static Pressure Analysis with Five-Hole Probe

In Treaster and Yocum,[32] the calibration and data processing procedure is explained in detail. In that procedure, five pressure readings from the probe are used to find total and static pressures. First, $C_{p,yaw}$, $C_{p,pitch}$, $C_{p,tot}$ and $C_{p,st}$ values are obtained from calibration process for each yaw and pitch angle combination. Then, pressure readings from each individual point in observation window are used to calculate $C_{p,yaw}$ and $C_{p,pitch}$ to give yaw and pitch angles of that point. If the coefficients give an intermediate value in calibration map, cubic interpolation [33] is used to find the exact angles. And then, corresponding $C_{p,tot}$ and $C_{p,st}$ values which are found in the calibration phase are used to obtain total and static pressure of the points. Again, cubic interpolation is used to obtain intermediate values of $C_{p,tot}$ and $C_{p,st}$. In the last step, velocity components are found by using the resultant velocity magnitude and yaw and pitch angles. The formulas are given below.

$$C_{p,yaw} = \frac{P_2 - P_3}{P_1 - \bar{P}}, \quad C_{p,pitch} = \frac{P_5 - P_4}{P_1 - \bar{P}}, \quad C_{p,tot} = \frac{P_1 - P_{tot}}{P_1 - \bar{P}}, \quad C_{p,st} = \frac{\bar{P} - P_{st}}{P_1 - \bar{P}}$$

$$\bar{p} = \frac{P_2 + P_3 + P_4 + P_5}{4}$$

$$\bar{V} = \sqrt{\frac{2}{\rho}(P_{tot} - P_{st})} \quad u = \bar{V} \sin\beta, v = \bar{V} \cos\beta \sin\alpha, w = \bar{V} \cos\beta \cos\alpha$$

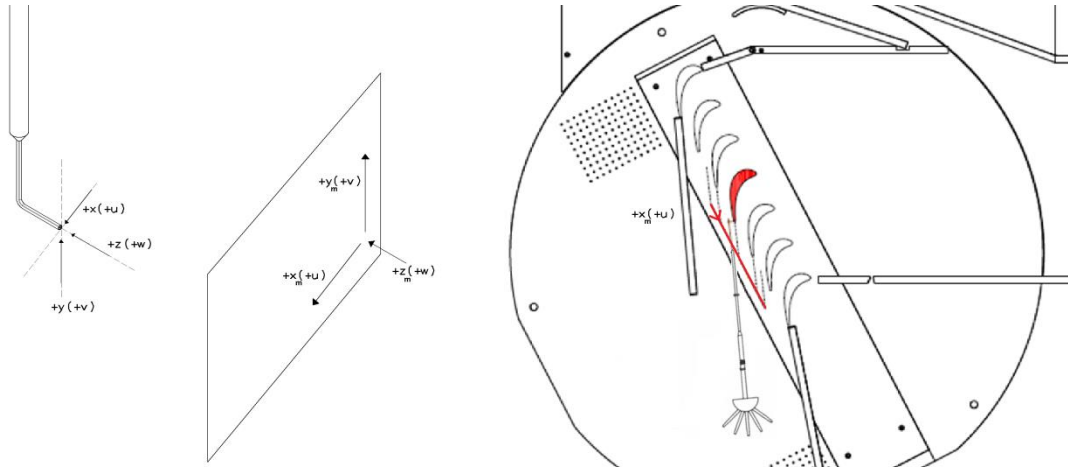


Figure 3. 1: Formulas of velocity components (left), positive directions of FHP and orientation on observation surface

After obtaining the total and static pressures, the pressure loss coefficients which are given in the Section 3.1.1 are used to quantify and compare the results. For velocity, vector plots and vorticity contours will be plotted.

3.1.3 Quantitative Evaluation of Measurement Results

For increasing the insight about the results, the blade passage averaged total pressure loss coefficient, $C_{p,m}$, will be calculated based on the high resolution data over a certain region for all three cases. In addition, the results of two sensors (Kiel and FHP) are also calculated and compared. In the Tables 3.1 and 3.2, the boundaries of calculation region and required pressure values are tabulated and graphically shown in Figure 3.2. Calculated $C_{p,m}$ values will be presented at the end of this chapter.

Table 3. 1: $C_{p,m}$ calculation window coordinates on observation surface

	X min (mm)	X max (mm)	Y min (mm)	Y max (mm)
Kiel Results	15	130	240	297,5
FHP Results	20	130	240	297,5

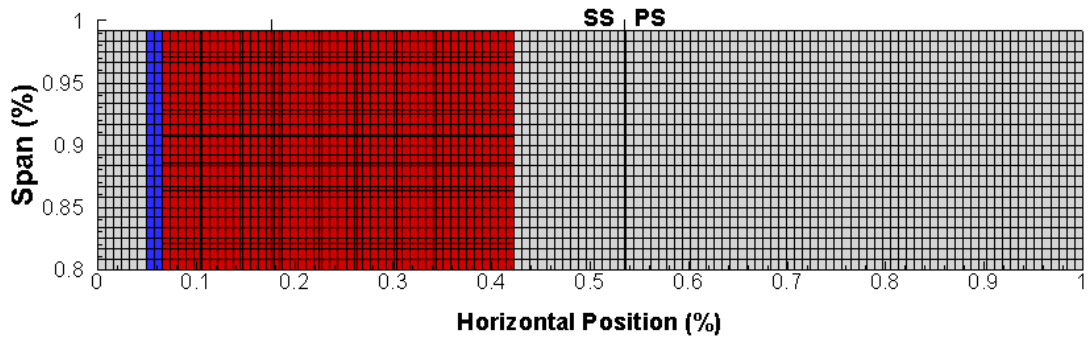


Figure 3. 2: The calculation window of $C_{p,m}$ on the measurement plane

For $C_{p,m}$ calculations with Kiel probe data, red section is used. However, blue section is also used with red section for $C_{p,m}$ calculations with FHP data. Because, the cubic interpolation method used to process the FHP data tends to give slightly more error in yaw angles. [33]

Table 3. 2: Required parameters for $C_{p,m}$ calculations

	U_{inf} (m/s)	P_{tot} (pa)	Density (kg/m^3)	P_{dyn} (pa)
For All Results	15.496	777.889	≈ 1.073	≈ 129

For calculation of improvement levels, following formula is used.

$$Improvement (\%) = \frac{C_{p,m,Flat} - C_{p,m,Squealer}}{C_{p,m,Flat}} \times 100$$

With this value, the reduction in pressure loss supplied by squealers is expressed by percentages with respect to the flat tip (reference) case. In this formula, $C_{p,m,Flat}$ is the $C_{p,m}$ value of flat tip case and $C_{p,m,Squealer}$ is the $C_{p,m}$ value of the squealers. The numerical results are given in Table 3.3.

3.2 Periodicity

In the scope of the periodicity controls, the tailboards are aligned with the last blades' surfaces (outer one with the pressure surface and inner one with the suction surface) and are positioned so that the wake regions at the downstream are tried to be similar. [Fig. 3.4]

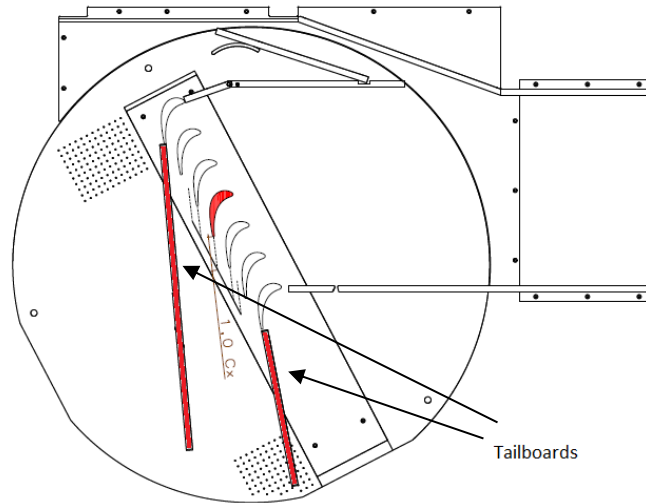


Figure 3. 3: A sketch of test section (top cover removed) and positions of tailboards

In Chapter 2, tailboards were shown as having the same length but later, the outer one is extended to reach nearly to inner one to reinforce the periodicity. Also, when bleed gates are open, total mass flow rate increases, hence the inlet velocity. But these are so sensitive that the balance of inlet velocity distribution gets easily disturbed by them.

After calibration and characterization works, total pressure measurements are carried out with flat tip blades at the 1 axial chord downstream for periodicity measurements. Two midspan heights are selected and measurements are done repeatedly. Figure 3.4 shows the results of measurements at the described plane. As can be observed, periodicity at the outlet is fairly achieved.

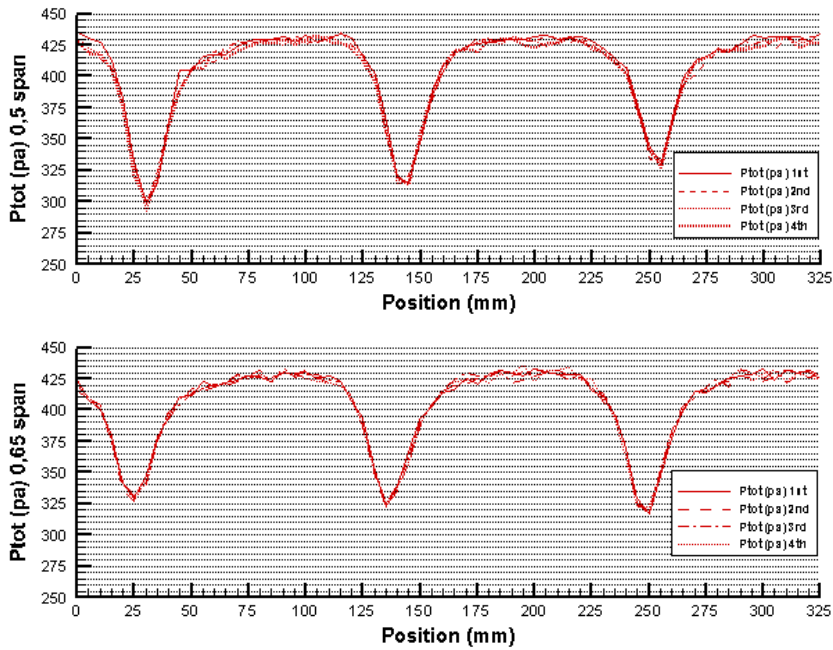


Figure 3. 4: P_{tot} measurements at 50% span (top) and 65% span (bottom)

3.3 Measurement Planning and Scenarios

The steps and main path to follow in tests are designed for understanding the basic physics of the blade passage flow and having the chance to investigate the main flow facts in detailed manner. Also, the effect of tip geometry on the characteristics of the TLV and other possible consequences will be observed. For this aim, three different blade tip geometries with the same blade profile will be used and whole results has been planned to be presented in two phases.

In first phase, total pressure measurements with Kiel probe are done with coarse step size, producing a low resolution data. This gives a low-density mapping in return of a wider region of observation. Bleed gates are kept open in an appropriate portion that it maintains the balance of both inlet velocity profile and exit pressure distribution.

These results will be presented in total pressure distribution contour plots. Then, observation region will be chosen smaller (if possible) with the knowledge obtained from low resolution data, then measurements are going to be done with finer step sizes with respect to the first case to produce high resolution data. Also, bleed gates will be closed fully this time and balance of inlet velocity profile and exit pressure distribution will be ensured. And these results will be presented in C_p contour plots.

In second phase, the calibrated five-hole will be used to obtain high resolution data. In this phase, velocity (flow angles, velocity components and resultant velocity) and vorticity information will be acquired along with total and static pressures all over the observation window. The bleed gates are kept as the same position with the high resolution case of Kiel probe. Results will be presented in C_p contour plots.

In both phases, three different blade tip geometries will be used. Flat tip geometry will serve as reference case and the others, partial and full squealer geometries, will be compared to reference case.

In this work, span and horizontal position are non-dimensionalized with span length (s) and three times of the pitch ($3*p$) respectively. The projection of the test blade will be marked on the observation region. More explanations and results regarding the measurements will be given in the following articles in appropriate sections.

3.4 Downstream Measurements with Kiel Probe

At downstream, measurements are done at 1 axial chord distance from trailing edge of test blade with Kiel probe. The cases and main planning is given at the following section.

3.4.1 Low Resolution Measurements

In low resolution measurements, identified observation window is scanned with 5 mm step size in horizontal and 15 mm step size in vertical direction. The width is 330 mm and the height is 150mm. These values correspond to +/- 1,5 blade passage width and 50%-100% span height.

This region is scanned with Kiel probe for three types of blade tip geometries. Flat tip is used as reference case and other two is compared to that case to determine the variations. Flat tip also shows the flow physics and can give an insight about the phenomena (TLV, PV, a possible CV) locations. With the help of this information, measurement plane can be narrowed down in second phase investigations.

3.4.1.1 Total Pressure Distributions

Flat tip case is the reference case in these measurements. The total pressure measurement results of this case are given in Figure 3.5 and suction and pressure sides of test blade and the blade's projection are shown on the measurement plane.

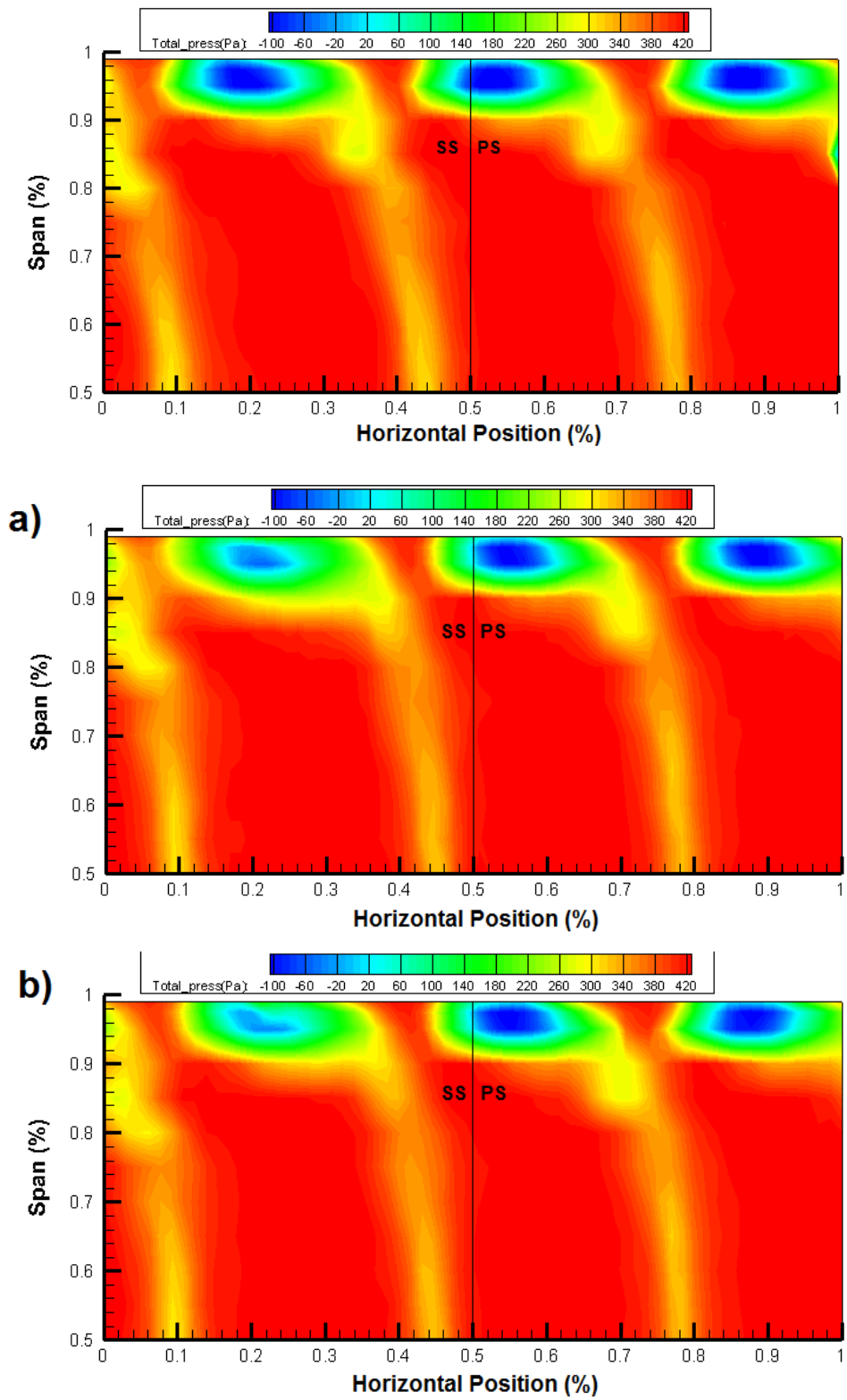


Figure 3. 5: P_{tot} distributions for flat tip (top), partial squealer tip blade (a) and full squealer (b) with Kiel probe in low resolution

The first inference from Figure 3.5 is that wake regions of two blades are clearly seen. In addition to that, periodicity is established fairly. In this distribution map, test blade's projection onto observation plane stands at 0.5 and the full wake which is roughly in between 0.1-0.5 belongs to the test blade. Besides, in this region, concentrated loss sections can be identified as explained in Chapter 1. In a broader sense, above 80% tip leakage related effects are dominant, below 80% it is understood that blade's wake effects are observed. The first region, above 80%, also can be divided into two subsections. Above 90%, there is a loss region called tip leakage vortex (TLV) and between 80%-90%, there is another loss region called passage vortex (PV) is visible. TLV is created at the tip corner of suction side than rolls and grows through suction side. PV is created from branches of HV of neighboring blades, these branches unite while moving in blade passage and shift through the suction side and tip region of the blade due to pressure difference inside the blade passage. (Refer to Chapter 1)

In Figure 3.5, there is an important event observed. The wake of the blade did not match with the projection of the blade because of boundary layer over the blades and tip leakage flow. This phenomenon is called as slipping and causes a reduction in total turning angle of blade. In turbomachines, total turning angle is an important design parameter of blades and any reason of reduction on this is not desired, since it affects the blade loading hence efficiency.

After flat tip, only the test blade in the cascade is changed with the blades which are having partial and full squealer geometries. Then, measurements are carried out at the same measurement plane with the same resolution levels. Results of these cases are given in Figure 3.5a and b.

When tip geometries are applied to blades, changes are observed in pressure distribution, center locations of the vortices and the area occupied by them. These changes are especially in the region above 80%, where tip leakage flow takes place. Also there seems a difference between partial and full squealer geometries. In order to observe and compare the levels of improvements quantitatively, investigations will

be carried out above 80% since there were no significant changes observed in below 80% span.

3.4.2 High Resolution Measurements

In high resolution measurements, observation window is shrunk to 80%-100% span height and 330mm width, which corresponds to 60mm in vertical and nearly 3 blade passages in horizontal direction respectively.

Also this time, step size is smaller hence the results are in high resolution. In both directions, step size is 2.5mm. And in addition, pressure loss coefficient (C_p) is calculated for all observation window and C_p distribution is given this time.

3.4.2.1 Total Pressure Loss Coefficient Distributions

As mentioned in the low-resolution results section, flat tip case is the reference case and the other cases will be compared to that.

The result belonging to flat tip case is presented in Figure 3.6. In the figure, test blade passage is marked and the difference based from tip geometry is expected to be observed in this section.

As similar to low resolution results, periodicity is established. At a first glance, one can identify two main vortex structures. In between 0.05-0.425 horizontal and over 90% vertical position, there is tip leakage vortex observable, marked with “TLV”. The other vortex structure, in 82%-88% vertical and 0.3-0.4 horizontal area limits, is the passage vortex and marked with “PV”. These vortex structures are observed distinctively and connection between them is weak in this case.

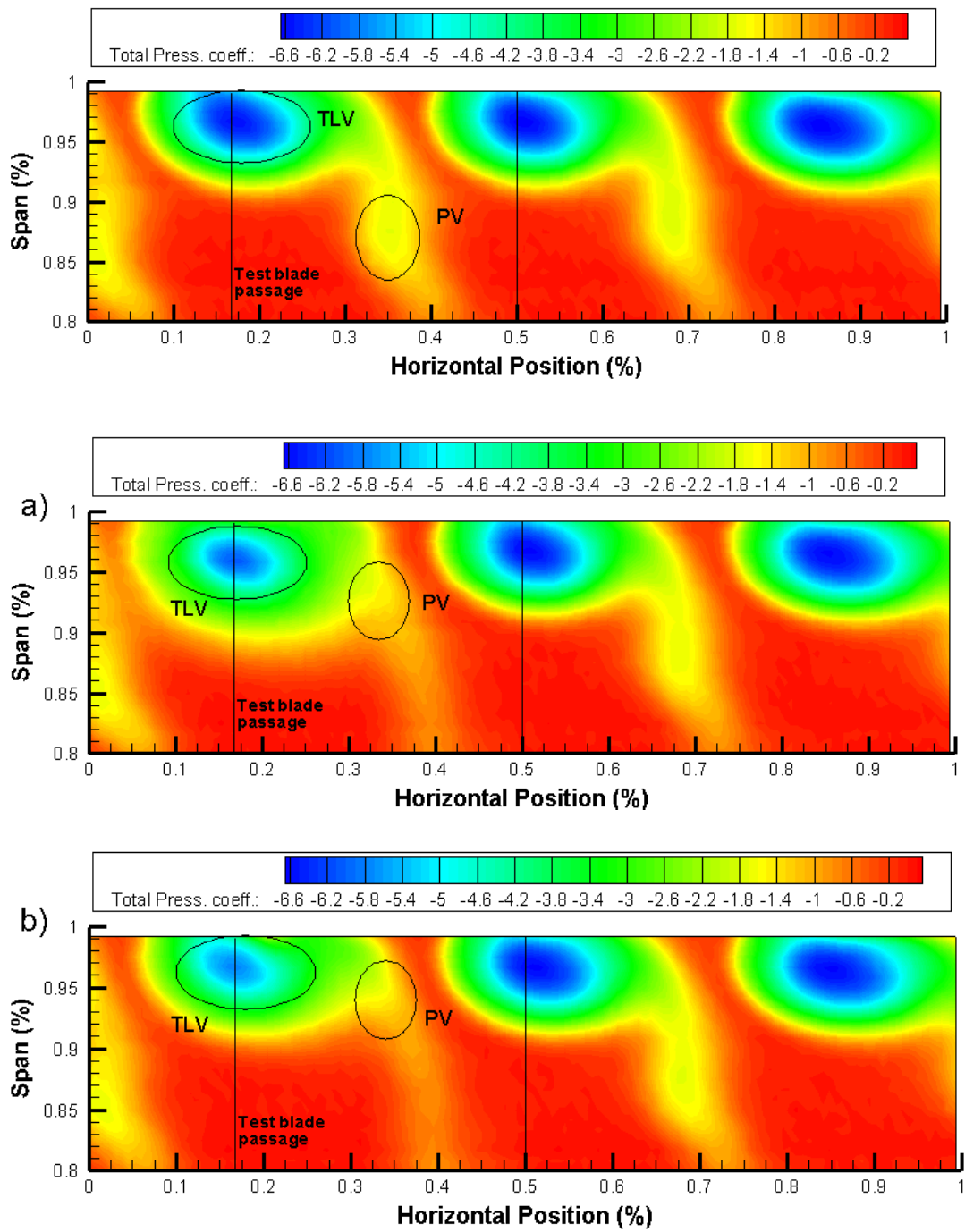


Figure 3. 6: Cp distributions for flat tip blade (top), partial squealer tip blade (a) and full squealer (b) with Kiel probe in high resolution

The other two different tip geometries are replaced with the center blade as planned in the previous section and measurements are carried out in the same observation window. Results are given in Figure 3.7a and b.

In Figure 3.6, TLV and PV are marked again and the behavior and changes are captured in a more detailed manner as planned. In first sight, it can be easily seen that in both cases, TLV is weaker and vortex core is smaller than the reference case which means using a tip geometry can help reducing the pressure loss caused by tip leakage. An effect of tip geometry is observed also on the PV. It is seen that the center of passage vortex is moving through TLV and probably getting weaker. Furthermore, the effects of the test blade are observable in regular blades' wakes.

In Figure 3.6a, it is seen that the TLV region is slightly bigger than reference case but the core is smaller. In addition, PV gets closer to the TLV with partial squealer geometry. That is probably because TLV loses its effectivity and PV finds chance to move through the TLV [17]. Since PV preserves some of its energy [22], it may transfer some of its energy to TLV and TLV region enlarges but still pressure loss is reduced. In addition, the center of the TLV moves slightly through the left and downward. [34], [35]

In Figure 3.6b, TLV region is in nearly same dimensions with the reference case and vortex center remains stationary but PV moves further through TLV. The movement of PV can be explained with the same reason as in the partial squealer case. And the re-shrinkage of the TLV region is due to total energy loss –and therefore vorticity intensity- of the whole vortex system. The vortex center does not change location but the total pressure loss decreases and vortex core gets smaller.

3.4.2.3 P_{tot} Investigation at the TLV

In Figure 3.7, the total pressure measurements of tip treatment cases are compared with reference case. The data in this graph belongs to the vertical cross section of the

TLV centers of each case which roughly corresponds to the 16.5% of the horizontal position. Data are extracted from the high resolution data and non-dimensionalized by dividing the inlet total pressure.

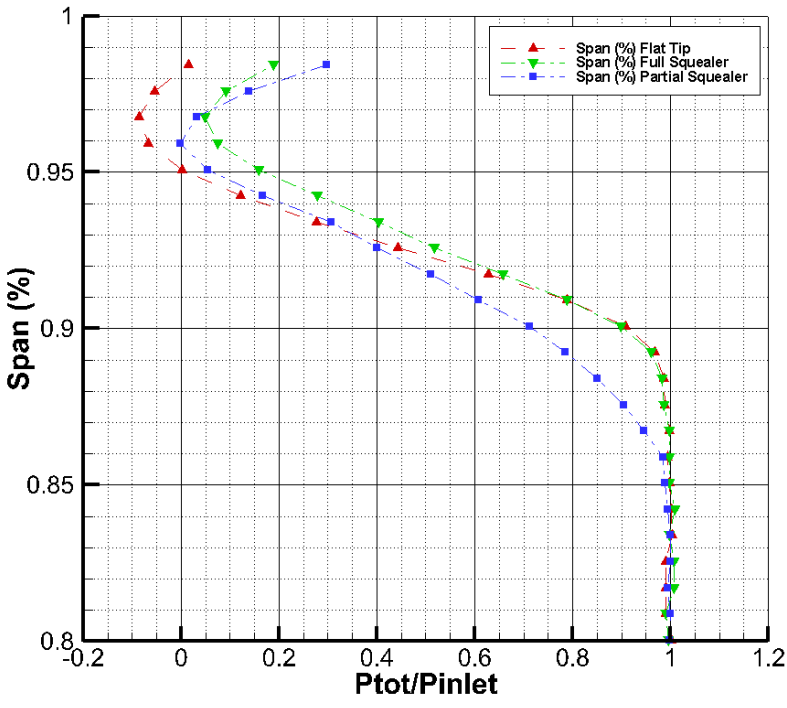


Figure 3. 7: Ptot/Ptot,inlet graph along 16,5% horizontal position

As it can be seen from Figure 3.7, the best performance of pressure loss reduction belongs to the full squealer tip case. Partial squealer case also gives some positive signs especially at around the center of the vortex but since the vortex area is the

widest in this case, the total pressure loss reduction is relatively low. In addition, flat tip case also has a significant PV region which is not seen in this graph.

This graph also tells that the vortex area is the largest in partial squealer case as indicated before.

3.5 Downstream Measurements with Five-Hole Probe

Five hole probe measurements are done at 1 axial chord downstream distance from trailing edge of test blade.

3.5.1 High Resolution Measurements

In high resolution measurements, observation window is shrunk to 80%-100% span height and 307.5 mm width, which corresponds to 60mm in vertical and nearly 3 blade passages in horizontal direction respectively.

Also, in both vertical and horizontal directions, step size is 2.5mm. And in addition, pressure loss coefficient (C_p) is calculated for all observation window and C_p distribution is given this time.

3.5.1.1 Comparison of Kiel Measurements with FHP Measurements

For comparison and consistency of the measurements, total pressure loss coefficient (C_p) distribution is computed from FHP measurements and given in Figure 3.8 and Kiel probe measurements are given in Figure 3.9. These distributions are also used to

find $C_{p,m}$ values for all cases in order to estimate the pressure loss level and compare the results of two measurement probes.

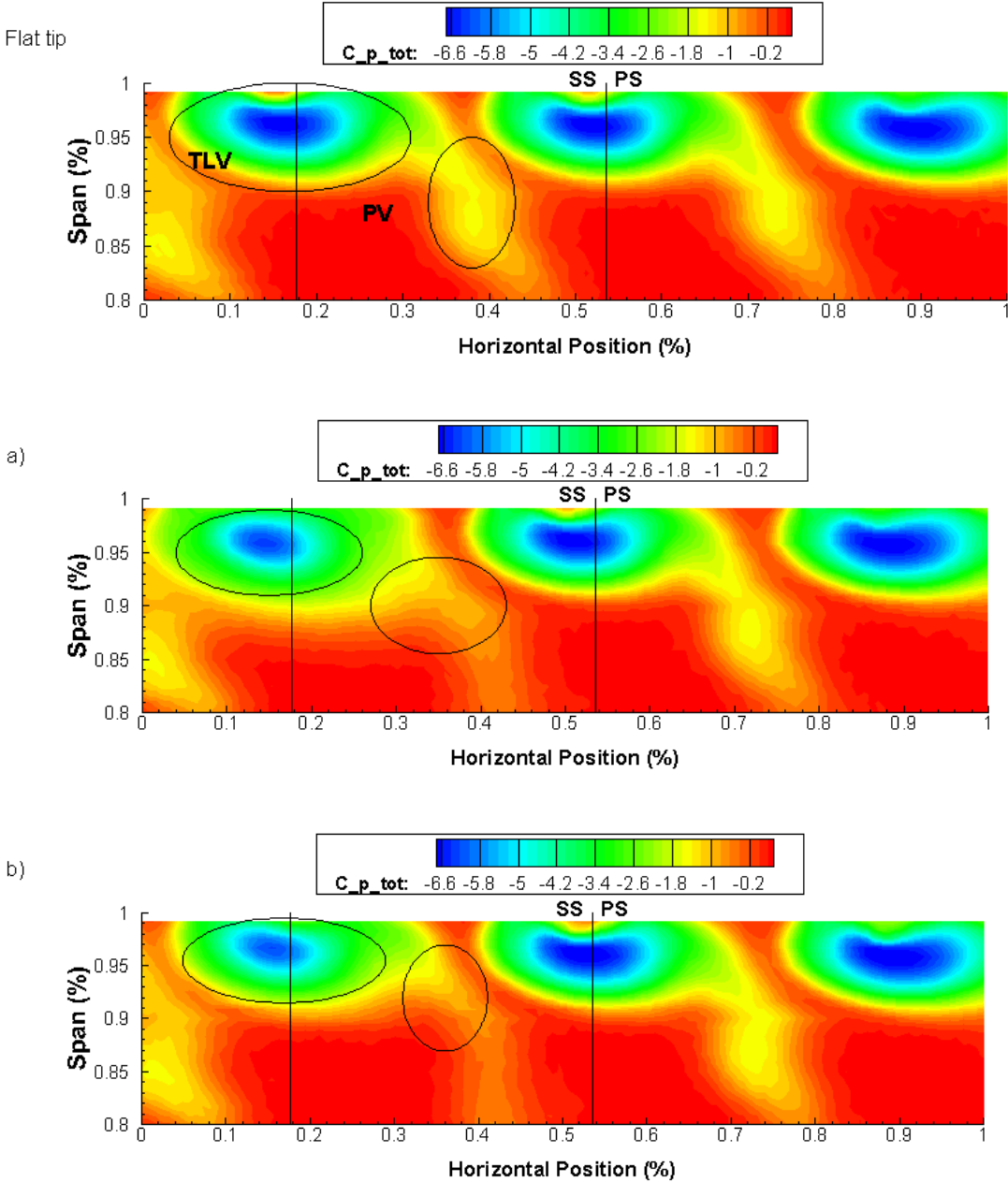


Figure 3. 8: C_p distribution for flat tip (top), partial squealer (a) and full squealer (b) with FHP measurements in high resolution

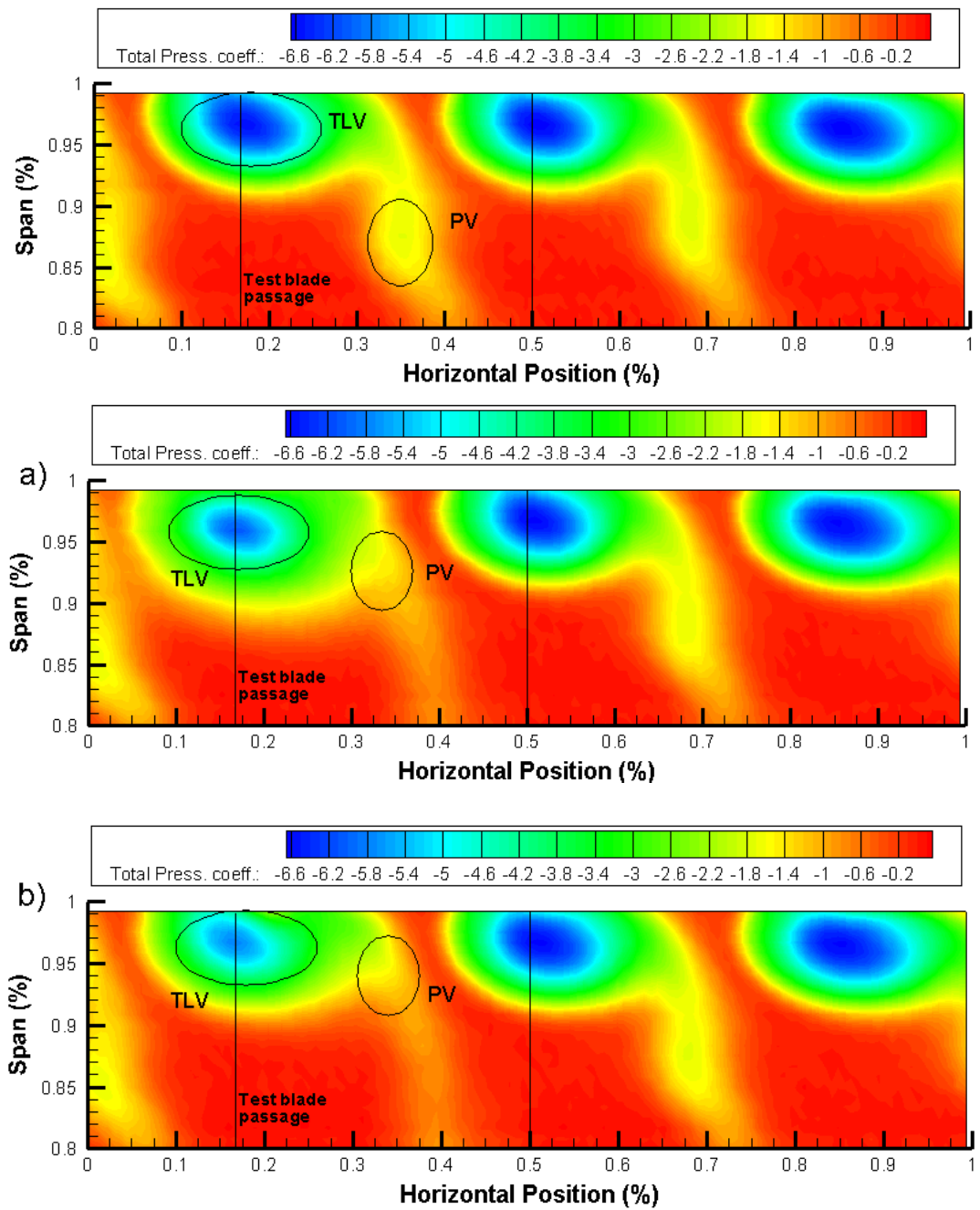


Figure 3. 9: C_p distributions for flat tip blade (top), partial squealer tip blade (a) and full squealer (b) with Kiel probe in high resolution

When the C_p distribution from FHP is compared to Kiel measurements, it is clearly seen that two methods give highly consistent data under the same conditions. In addition, two vortices show same behavior in all measurements with changing blades, TLV and PV are getting weaker and PV is moving through the TLV core. The strength of PV is measured as a slightly lower value than Kiel in FHP.

However, there are two points observed in Figure 3.8 which are interesting. First, TLV core changes from a more circular shape in Kiel to a bean-like structure in FHP. When the previous literature works are studied, it is seen that the TLV gets wider with the FHP utilization. As an example, similar bean-like structure reported by Nho [36] is given below.

In the study of Nho, a FHP is used to collect data from the measurement window. The grayscale in the Figure 3.10 shows the C_p distribution and from top to down tip clearance is 0%, 1,5% and 2,3% respectively. At the top figure, no TLV is observed since tip clearance is zero and the vortex marked with “A” is PV and vortex marked with “B” is trailing edge separation vortex. And in the middle and bottom figures, TLV is marked with “C”. As the grayscale shows, TLV has a bean-like distribution.

The second interesting point is the “dents” at the top of each blade wake in FHP measurements. Again from the literature, it is seen that the typical calibration angle interval of FHP is around $\pm 40^\circ$ for this type of experiments. In addition, the positioning of the probe with the measurement plane can create problems.

In our work, the FHP calibration setup was only available up to $\pm 27^\circ$ due to physical constraints of setup structure. And in measurements, if the flow happens to come with an angle larger than this, code applies some extrapolation but error margin increases with increasing difference in angles. In addition, positioning of the probe with measurement plane is a source of error. The FHP is aligned with the streamwise direction while measurement plane is along the pitchwise direction. Then, projections of the vortices and velocity vectors are observed on the measurement plane. When this positioning issue is combined with the calibration angle interval problem, cause a failure and manifest as these dents. In the given example study of

Nho, the tip section reaches 95%-96% span, at most. But in our work, FHP tried to be put as close as possible to the top casing wall. To avoid this error, these sections were masked in literature.

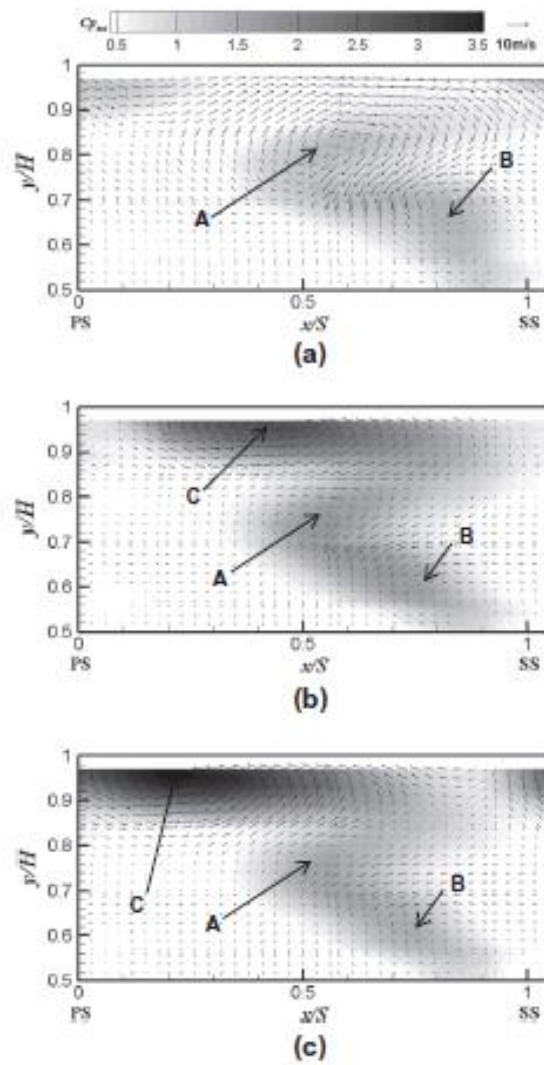


Figure 3. 10: C_p measurement (in grayscale) of Nho[36]

The $C_{p,m}$ results will be given in Table 3.3 and a more complete evaluation and comparison will be made there.

3.5.1.2 Collective Results

The reference case is flat tip blade and the P_{tot} distribution and velocity vectors will be given in the following series of figures.

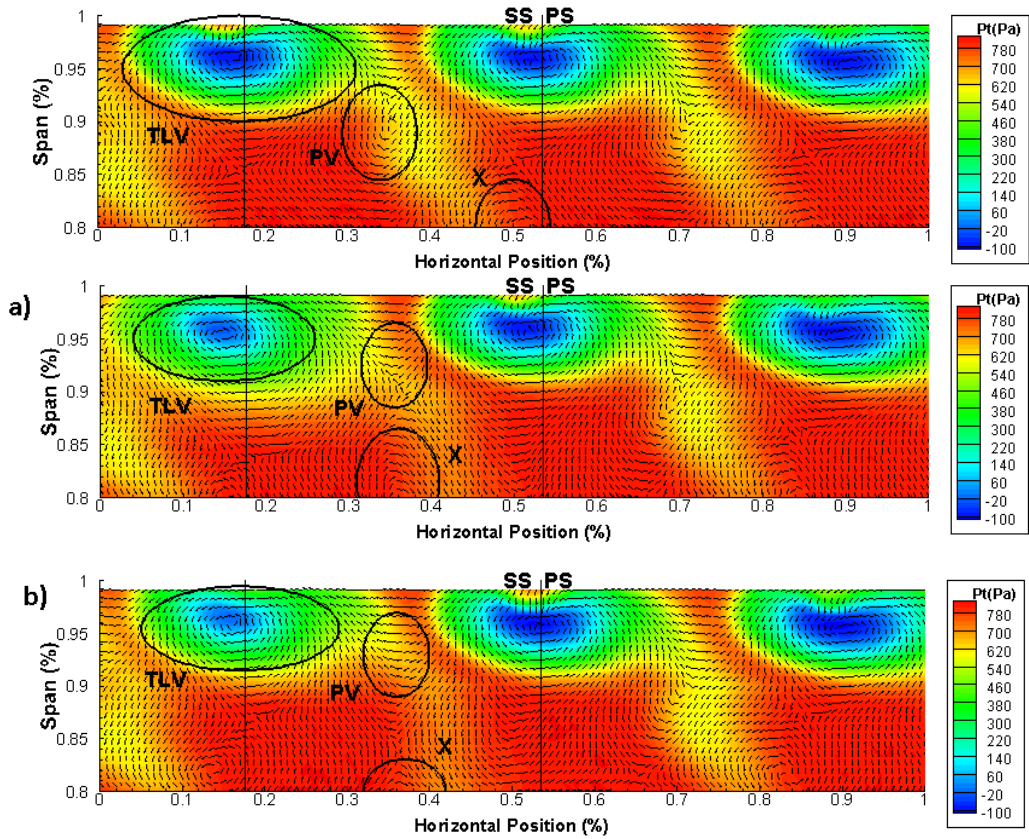


Figure 3. 11: P_{tot} and velocity vectors for flat tip (top), partial squealer tip (a) and full squealer (b) cases

As can be seen from the Figure 3.11, TLV and PV are observed at their expected sites. In addition, high pressure loss locations are matching with the vortices. But when the measurement region is investigated in detail, it is seen that there is a new vortex structure has emerged. It is marked with X in the graph. This observation is made possible by the five hole probe since velocity vectors made that new vortex visible. A similar structure is reported by Nho and Yamamoto [36] in their separate researches. Nho reports from Yamamoto about this structure as “A counter clockwise rotating vortex near the passage vortex is the trailing edge separation vortex which is caused by the separation of the passage vortex at the trailing blade edge.” This structure is also periodic (appears also ~15% and ~85%) in flat tip blade and coincides with the blade wake region below 80% span which is not in the range of this measurement but it can be observed from the low resolution data. However, according to Langston, this structure is Counter Vortex and is created by the suction side branch of Horseshoe Vortex. Since upstream measurements were not done, the main reason behind that structure is not fully clarified.

The results belonging to partial squealer and full squealer tip geometries are given in Figure 3.11 a and b. In these figures, it is clearly seen that TLV gets weaker and total pressure loss is reduced. The PV is observable but it could be better visualized if a finer step size was used. Nevertheless, the PV migration under the flow field effects is observed. PV migration can also be seen from the vorticity contour plots. [Fig. 3.11]

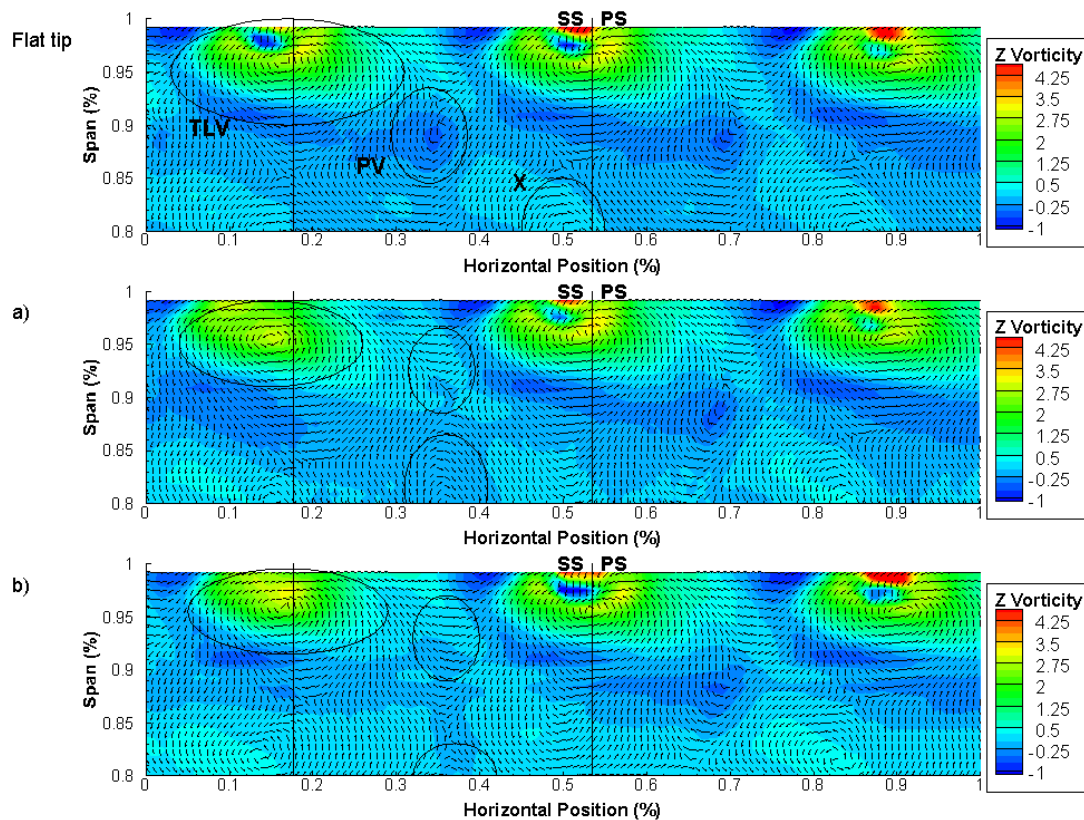


Figure 3. 12: Vorticity and velocity vectors for flat tip (top), partial squealer (a) and full squealer (b)

Vorticity plots [Fig. 3.12] show that, for all squealer geometries, TLV nearly retains its vorticity level and vorticity level of PV drops. The change in TLV manifests as an effective area reduction. When partial squealer tip is used, TLV loses its effective area and migrates through TLV. And vortex X also travels in horizontal direction and enlarges in vertical.

And in full squealer case, the effective area of TLV reduces further and PV travels further through TLV. But the interesting point is that vortex X does not migrate towards the section left by PV. Normally, the expected action is that the vortex X should move through there since other vortices are getting weaker than the flat tip

case. In addition, when the sense of the vortex X is investigated in detail, it is seen that the vortex X changes its direction with squealers. For observing this and seeking for a reason, streamline graphs are plotted for all cases. [Fig. 3.13]

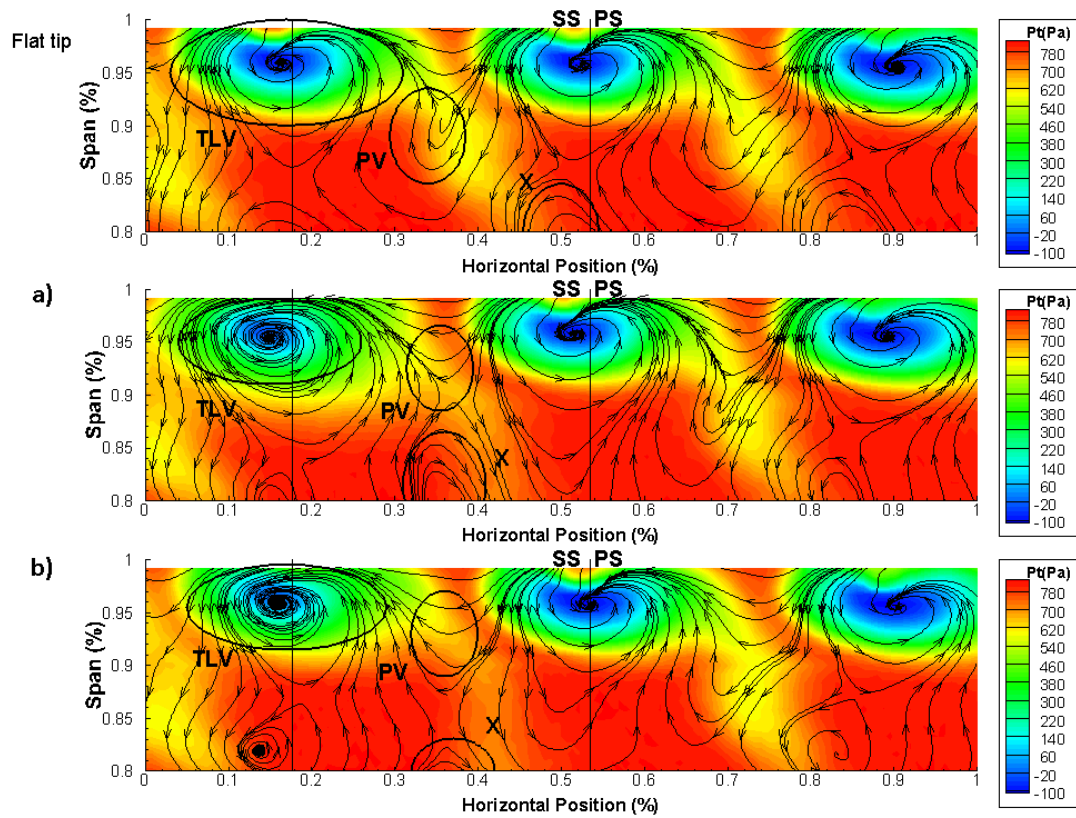


Figure 3. 13: P_{tot} and streamlines for flat tip (top), partial squealer (a) and full squealer (b)

From the streamline plot [Fig. 3.13], we can see that when PV moves upward, vortex X becomes exposed to the force of the neighboring TLV. In partial squealer case, PV

is not gone too much through TLV; hence, it protects the vortex X a little and vortex X also moves through PV. However, in full squealer, TLV and PV are in their weakest positions and vortex X takes the effect of neighboring TLV fully. This way, the sense of the vortex X changes because neighboring TLV breaks all the connection of the vortex X with the PV and alters the sense. This behavior can be clearly observed just by following the streamlines of the neighboring TLV and this is thought to be the reason for the altered sense of vortex X.

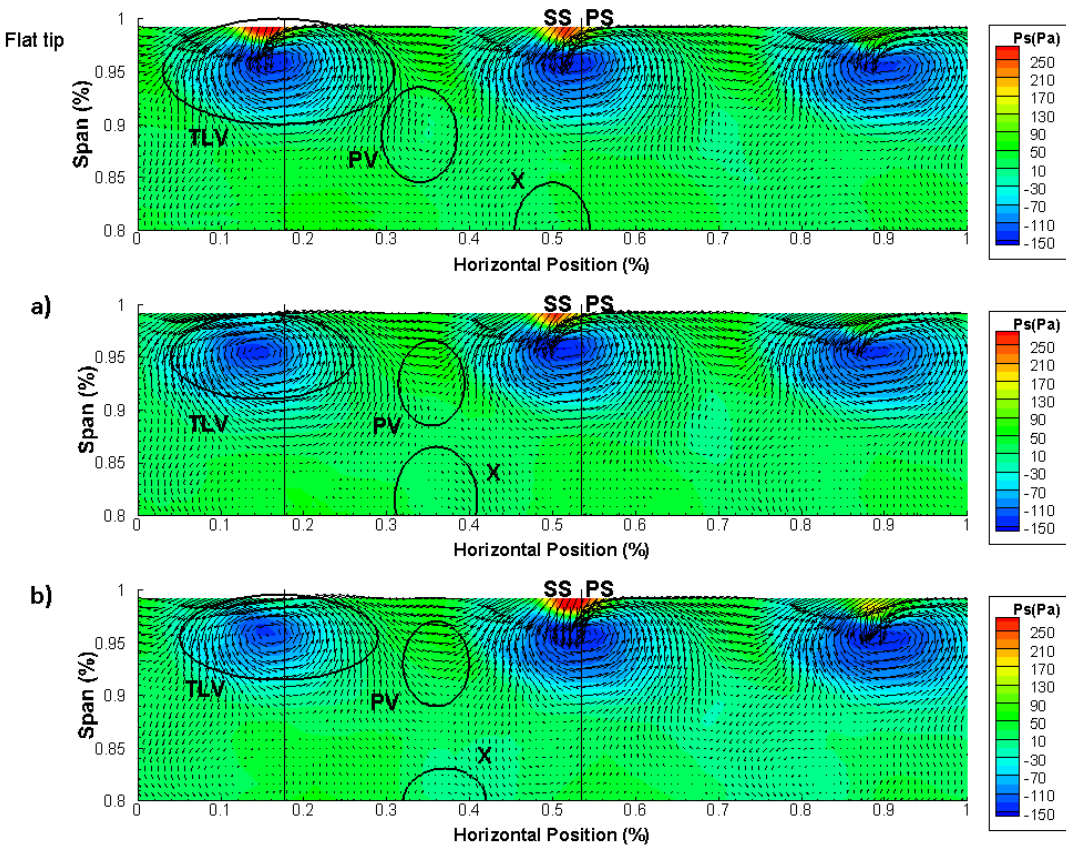


Figure 3. 14: P_{st} and velocity vectors for flat tip (top), partial squealer (a) and full squealer (b)

In Figure 3.14, static pressure distribution and in-plane velocity vectors are given in contour plots and vector plots respectively. It is seen that lowest Pst peaks coincide with the TLV cores as expected and PV and vortex X have their traces on the distribution. Since vortices lose their strength, a reduction of effective area is observable. A more detailed assessment about this topic will be done.

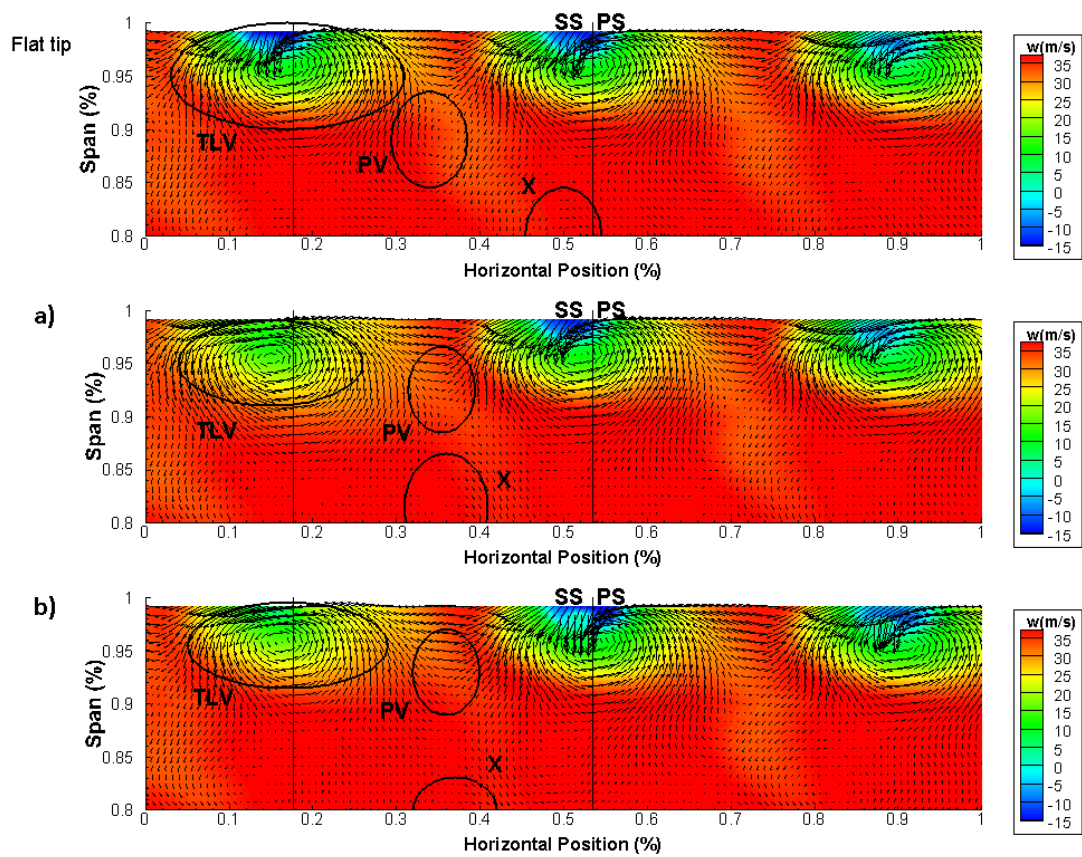


Figure 3. 15: 3 velocity component vectors for flat tip (top), partial squealer (a) and full squealer (b) (out-of-plane component (w) given with contour plot)

In Figure 3.15, all three velocity components are given. In plane velocity components are drawn in a proportional scale to real velocities and out-of-plane velocity component is given as contour plot. It is clearly seen that periodicity is good. In addition, the tip geometries produce an observable change over the velocity field. In flat tip blade, it is seen that tip jet is in strongest position and partial and full squealers are straighten and reduce the strength of tip jet since the in-plane and out-of-plane vectors get smaller. So, this means that the mass flow rate of the tip jet is reduced with the squealers and the consequence was observed in the total pressure distribution as effective area reduction of TLV. Also, the blue region which shows that there is a negative velocity (backflow) at the tip region is a sign of the error mentioned at Section 3.5.1.1.

For detailed investigation, five horizontal lines at different spanwise locations used to extract data in pitchwise direction and the graphs are plotted. The numerical values are non-dimensionalised by U_{inf} , $P_{st,exit}$, $P_{tot,exit}$ which are 15,496 m/s, 37,6188 Pa and 794,6144 Pa respectively. And for the magnitude of resultant velocity vector, Q is found from total and static pressures of the measurement point and also non-dimensionalized. For pressures, the values at exit are used since these measurements are done at that location.

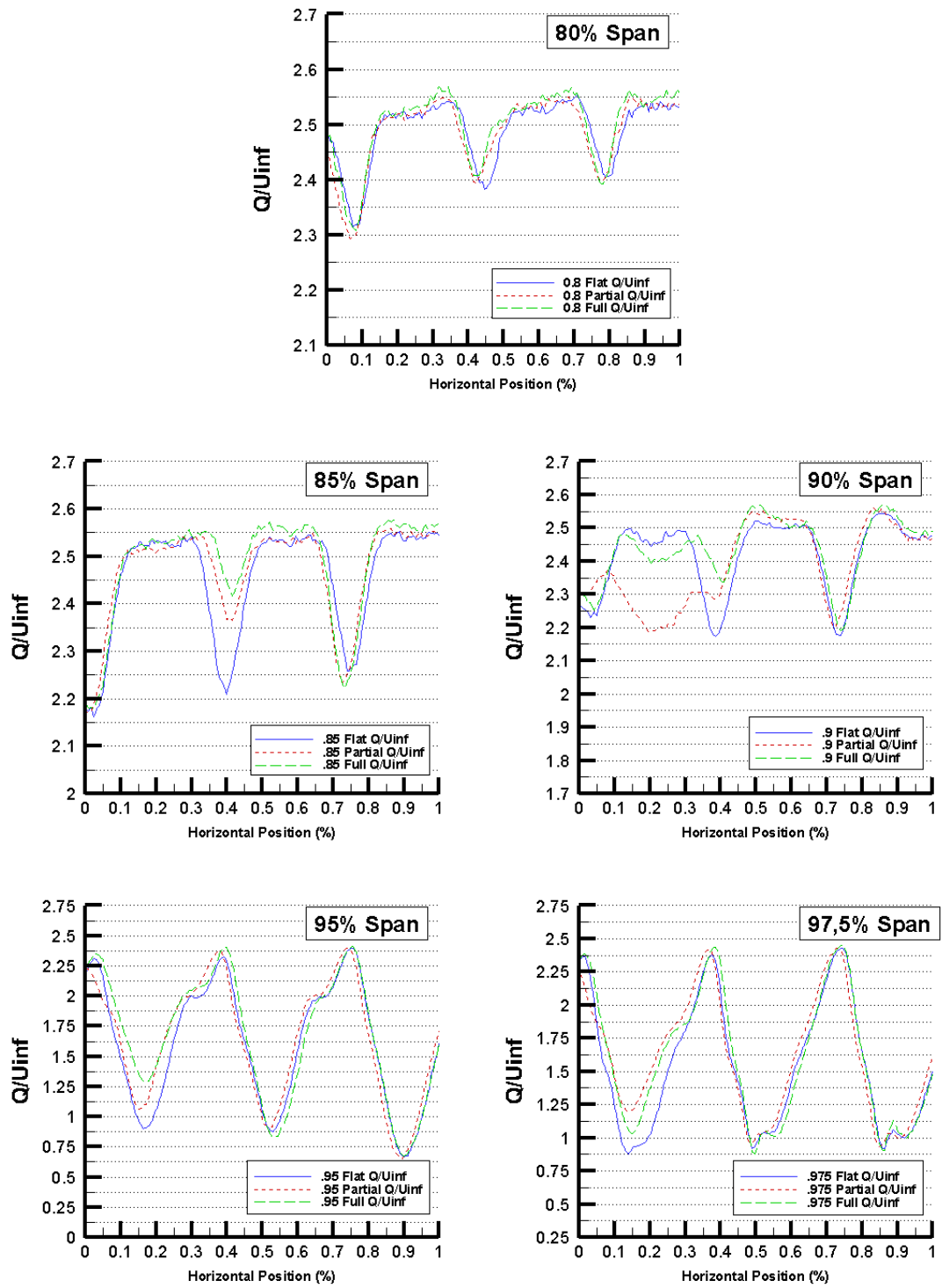


Figure 3. 16: Q distributions along pitchwise direction at different span levels

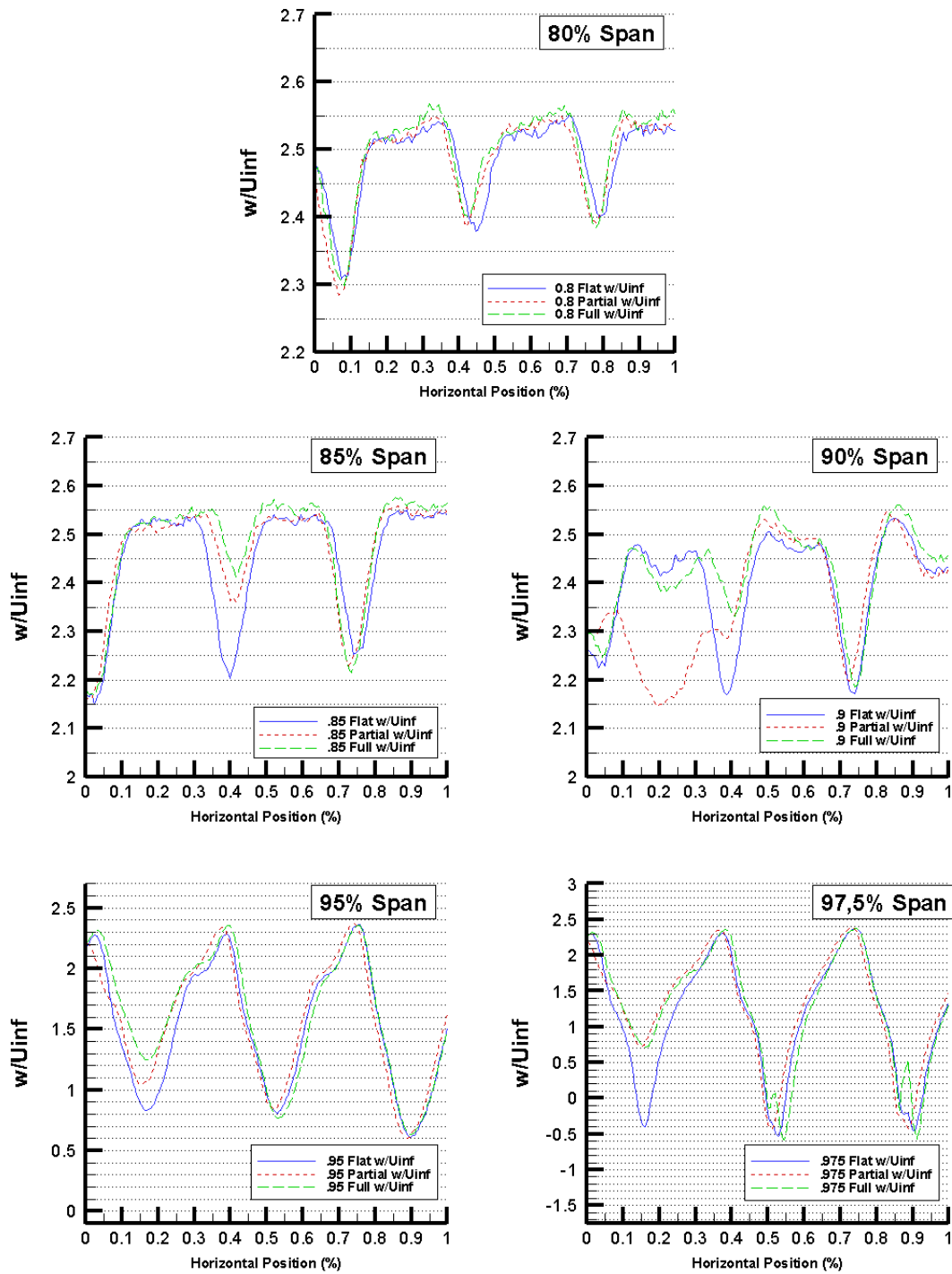


Figure 3. 17: Streamwise velocity component (w) distributions along pitchwise direction at different span levels

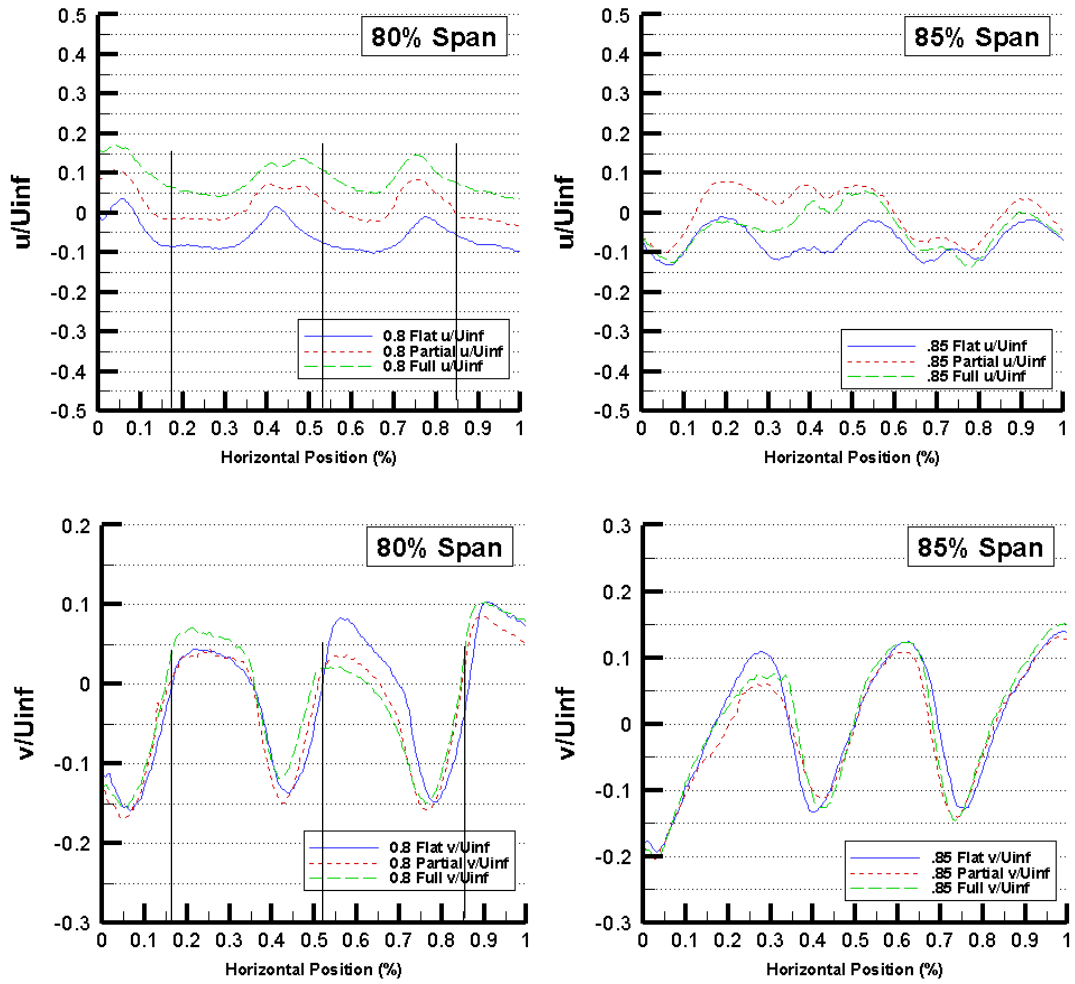


Figure 3. 18: u and v velocity component distributions along 80% and 85% span levels

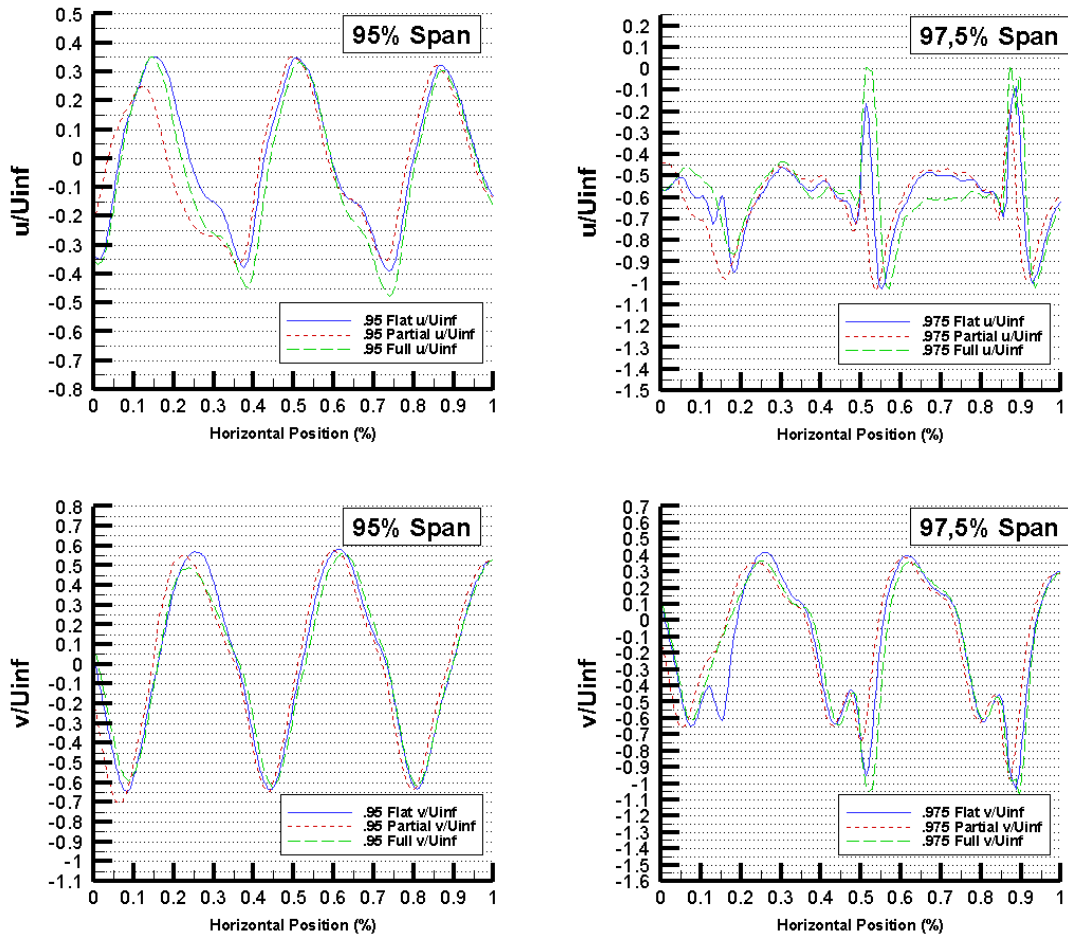


Figure 3. 19: u and v velocity component distributions along 95% and 97,5% span levels

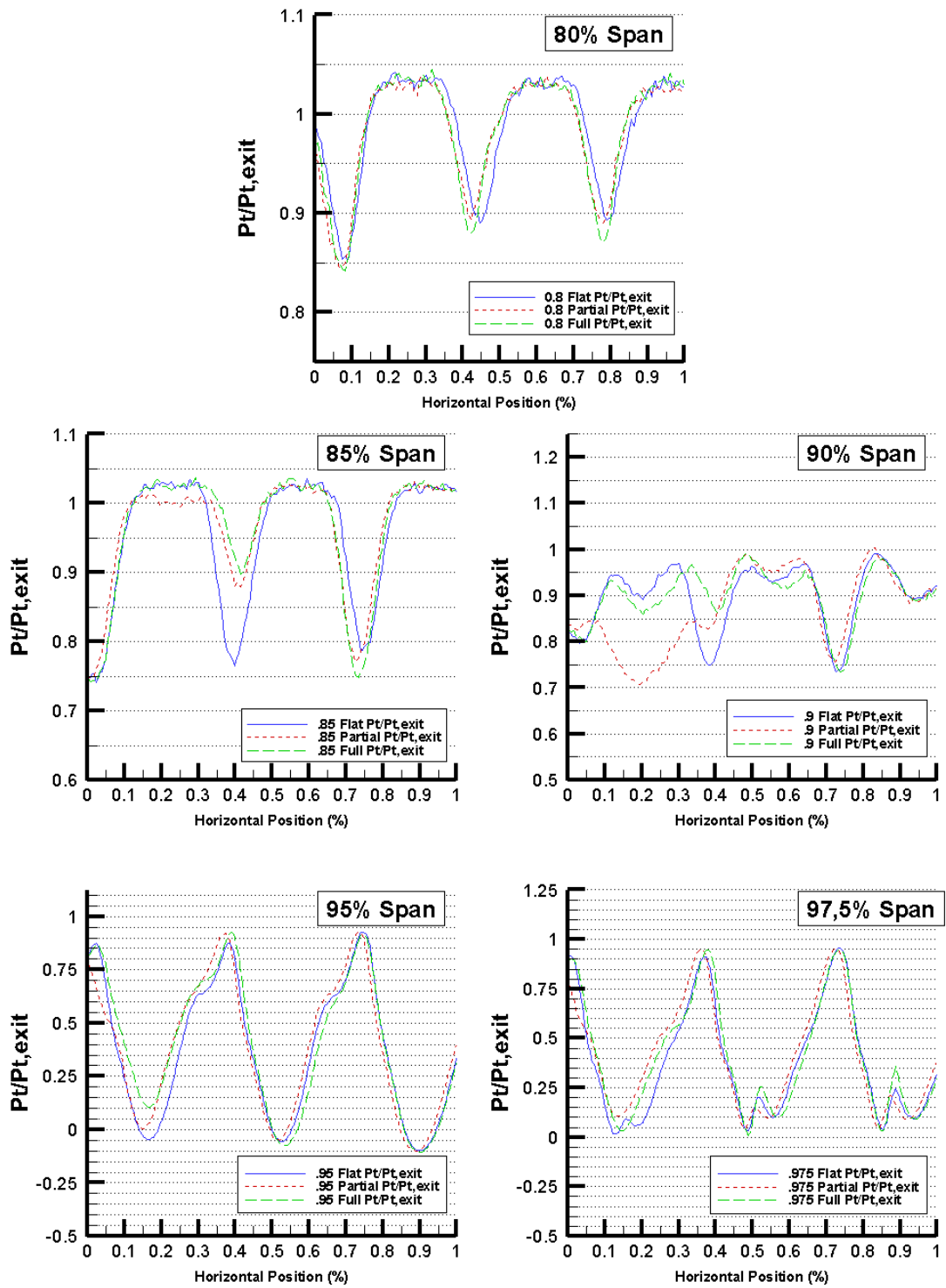


Figure 3. 20: P_t distributions along pitchwise direction at different span levels

These graphs are plotted in 80% (blade wake), 85%, 90% (PV), 95% (TLV), and 97,5% (tip clearance) span locations in pitchwise direction and values are non-dimensionalised with proper figures. In Figure 3.16 and 3.17, velocity defects normally exist in 80% span due to blade wake and no effect of tip geometries is observed in this span level. In addition, effect of the u and v components on Q are very limited since Q and w distributions show very similar trends. At 85% span, squealer geometries recover velocity defect in a considerable amount since PV moves in vertical with squealers, and in these, full squealer is observed to be more effective. This means, main flow velocity or closer velocity levels are obtained also at higher sections. In 90% span, it is known that velocity defect is due to PV in flat tip case (also a small contribution from TLV), but since effective area of TLV becomes larger with partial squealer, velocity distribution gets affected by TLV even at 90% level of span. And since PV moves towards TLV with squealers, velocity defect recovery at PV section is observed in 90% at the same time. The same velocity defect recovery effect is observable in higher span levels due to weakening of the TLV.

In Figure 3.18 and 3.19, u and v components of the velocity are given. u and v are in-plane velocity components and give a detailed idea about the vortices. u and v belong to horizontal and vertical components respectively and positive directions are given in Figure 3.1. In 80% span, there are some significant alterations observed but these are thought not to be in connection with tip geometries. When detailed investigations (vertical lines show the position of X) are done, it is seen that u and v -velocity distribution show meaningful variations in correlation with vortex X at 80%. These graphs mainly show that the lower span locations are in control of main blade passage flow direction since variations in u - and v -components are very limited and in higher span locations (above 90%), velocity field takes shape according to the vortices.

In Figure 3.20, P_t distributions are plotted. When P_{tot} graphs are examined, there is no effect of tip geometries observed at the 80% span. But when higher span locations are examined, the positive changes due to tip geometries on pressure distribution are

clear. At each span level, tip geometries perform better than flat tip and full squealer is observed as the best tip geometry in all span levels. At 90% level, the enlargement of the TLV with squealer shows its effect on total pressure distribution, as it was observed on velocity distribution before.

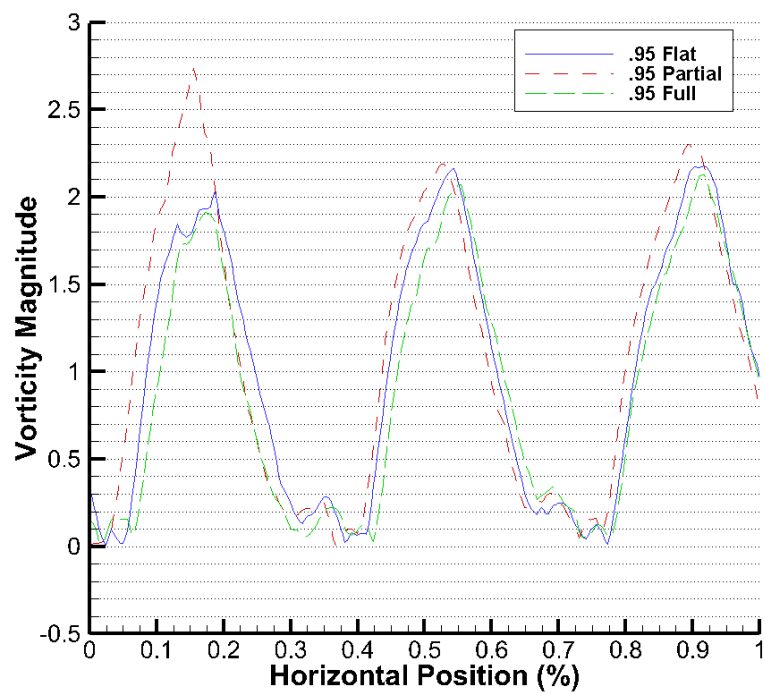


Figure 3. 21: Vorticity magnitude along the 95% span level

In Figure 3.21, out-of-plane vorticity magnitude is given at the 95% span level. As it can be observed from the graph, full squealer has the lowest magnitude and partial squealer has the highest.

Table 3. 3: Results of Kiel and FHP measurements and improvement percentages

	$C_{p,m}$ (Kiel Probe)	$C_{p,m}$ (FHV Probe)	Improvement (%) (Kiel Probe)	Improvement (%) (FHV Probe)
Flat Tip	-1.459544	-1.360669	(reference)	(reference)
Full Squealer	-1.169466	-1.101055	+19,87	+19,07
Partial Squealer	-1.411199	-1.343336	+3,31	+1.27

As it can be seen from Table 3.3, both squealers give positive improvements as expected from the test results and previous literature. The only thing is, for this blade profile, full squealer configuration gives far better performance than partial squealer. Partial squealer configuration gives similar pressure loss behavior with the full squealer around the center of the TLV.(Figure 3.6) But, since partial squealer produces a larger TLV (compare Figures 3.8 and 3.9 / refer to Figure 3.20 90% span), has a more distinct PV region than full squealer (Figure 3.8-a-b and Figure 3.9-a-b) and has higher vorticity levels (refer to Figure 3.21), partial squealer performance is not as good as full squealer. However, since the effectiveness of partial squealer around the TLV is similar to full squealer, a better performance than this was expected.

Also there is no big difference between the Kiel and five hole measurements. The general trend is FHP estimates a lower improvement level for both cases. This might be due to the differences in working principles or measurement errors of the probes or calibration inaccuracies of the FHP. In addition, the cubic interpolation which is used in calibration procedure tends to give a higher error in yaw angle plane. [33]

CHAPTER 4

CONCLUSION

The aim of this thesis was to investigate the efficiency losses due to tip leakage vortex (TLV) in linear cascade by using experimental methods. For this purpose, the mechanism behind the flow phenomena is observed and from many active and passive flow control methods (FCMs), partial and full squealer tip geometries were applied, which are types of passive FCM. These tip geometries were designed and applied to a high pressure turbine blade and the results were compared with the blade with a flat tip. In linear cascade which includes 7 blades, the middle blade was chosen as the test blade and these blades were mounted interchangeably. Inlet and outlet flow measurements were carried out with Pitot - static tube, Kiel probe and single sensor Hot wire. Outlet measurements were done at the 1 axial chord downstream of blade row. As a result, total pressure distribution and pressure loss coefficients were obtained from measurement.

In experiments, measurements were divided into two categories, low resolution and high resolution measurements with Kiel probe and high resolution measurements with FHP. Low resolution measurements were done with less measurement points in a larger area, showed main trends of the flow and vortices and the main region needed to be investigated more carefully. High resolution measurements were done with more points over a smaller region and gave possibility to investigate the changes in more detail. Then, measurement window is shrunk to that section and resolution was increased. In these categories, flat tip case served as both reference

case and gave an idea about the structure of vortex mechanism and displacements. Other two cases, partial squealer and full squealer cases will be compared to the reference case and performance levels were calculated.

When reference case and the other two cases were examined in low resolution Kiel probe measurements, it was seen that there were traces of three distinct regions exist in P_{tot} distribution contour plots. These are tip leakage vortex (TLV), Passage vortex (PV) and the top section of blade wake. In addition, these vortices are strongly interacting to each other and changing their core locations with the different tip geometries. The essential alterations took place at the top 20 percent span in these vortex structures in the low resolution data. In high resolution results, TLV occupied a bigger region in partial squealer tip geometry than reference case but it nearly returned to its original dimensions in full squealer. In addition, pressure loss magnitude of the TLV center core decreased in squealer cases with respect to the reference case, but full squealer performed better than partial squealer. Also PV lost its intensity and PV core moved through the TLV since TLV got weaker.

In FHP measurements, there is another vortex emerged at the region where the regular blade wake coincides. This vortex is identified from previous literature (Nho and Yamamoto) and named as vortex X and its mechanism and migration is also investigated. In reference case, it is observed as a periodic vortex as TLV and PV but in squealer cases, it migrates and rotation sense changes. When these events are investigated further, it is observed that vorticity levels of TLV and PV decreases and their locations changes, these changes make vortex X to become exposed to the effect of neighboring TLV. The developments in TLV and PV are again observed in FHP measurements.

As a result of these experiments, using a squealer geometry produced a better performance and between these, full squealer gave the best result.

As limitations of the study, linear cascade section, inlet Ma levels and different Re for high and low resolution measurements can be pointed out. Linear cascade section eliminates the rotational effects which are present at the actual turbomachine.

However, as discussed in the Section 2.2, for these types of experiments, linear cascades produce fairly satisfactory results under certain assumptions. In addition, in rotating turbomachine, the relative motion of blades to the stationary casing wall makes TLV weaker since this motion reduces the tip clearance mass flow rate. [37],[38] And, at the inlet, the velocity used in the experiments is around 4,5% of the speed of sound (Ma 0,045). This level is not even close to the actual velocity levels of the second stage HPT but in literature, these velocity levels are commonly used.[22], [25], [30]

In our experiments, inlet velocity distribution and turbulence intensity is tried to be kept as the same and balanced and flow uniformity was protected. Due to these reasons, inlet velocity was kept constant and weather conditions played an important role on changing of Re. But, this amount of change in Re in the literature is reported in literature as no reason of drastical changes in the character of vortex system.[31]

In the future, the scope of this work can be enlarged by studying some other topics in order to improve and produce more detailed results, which can be listed as,

- 1- Testing pressure side squealers also.
- 2- Using an active FCM along with the recent method or by itself.
- 3- Comparing active FCM schemes with Passive FCMs by conducting experiments.
- 4- Measuring blade surface static pressure distribution in different span locations.
- 5- Observing the top casing and blade tip surface streamlines. The tip gap flow mechanism can be fully understood.
- 6- Enlarging the five hole probe measurement interval in spanwise direction. The new emerged vortex structure (vortex X) cannot be identified precisely with this observation window.
- 7- Changing at least middle 3 blades with the treated tip blades.

REFERENCES

- [1] D. K. Van Ness II, T. C. Corke, and S. C. Morris, "Stereo PIV of a Turbine Tip Clearance Flow with Plasma Actuation," *AIAA Aerosp. Sci. Meet. Exhib. Reno, Nevada*, no. January, pp. 1–21, 2007.
- [2] O. P. Sharma and T. L. Butler, "Predictions of Endwall Losses and Secondary Flows in Axial Flow Turbine Cascades," *J. Turbomach.*, vol. 109, no. 86, p. 229, 1987.
- [3] S. A. Khalid, A. S. Khalsa, I. A. Waitz, C. S. Tan, E. M. Greitzer, N. A. Cumpsty, J. J. Adamczyk, and F. E. Marble, "Endwall Blockage in Axial Compressors," *J. Turbomach.*, vol. 121, no. 3, pp. 499–509, 1999.
- [4] J. D. Denton, "The 1993 IGTI Scholar Lecture: Loss Mechanisms in Turbomachines," *J. Turbomach.*, vol. 115, no. 4, p. 621, 1993.
- [5] Y. S. Li and N. A. Cumpsty, "Mixing in Axial Flow Compressors: Part I - Test Facilities and Measurements in a Four Stage Compressor," *J. Turbomach.*, vol. 113, no. 1, pp. 161–165, 1991.
- [6] Y. S. Li and N. A. Cumpsty, "Mixing in axial flow compressors: part II - measurements in a single-stage compressor and a duct," *J. Turbomach.*, vol. 113, no. 2, pp. 166–174, 1991.
- [7] R. Mailach, I. Lehmann, and K. Vogeler, "Rotating Instabilities in an Axial Compressor Originating From the Fluctuating Blade Tip Vortex," *J. Turbomach.*, vol. 123, no. 3, p. 453, 2001.
- [8] S. G. Azad, J.-C. Han, and R. J. Boyle, "Heat Transfer and Flow on the

- Squealer Tip of a Gas Turbine Blade,” *J. Turbomach.*, vol. 122, no. 1, pp. 725–732, 2000.
- [9] C. S. Tan, I. Day, S. Morris, and A. Wadia, “Spike-Type Compressor Stall Inception, Detection, and Control,” *Annu. Rev. Fluid Mech.*, vol. 42, no. 1, pp. 275–300, 2010.
- [10] H. Wu, D. Tan, R. L. Miorini, and J. Katz, “Three-dimensional flow structures and associated turbulence in the tip region of a waterjet pump rotor blade,” *Exp. Fluids*, vol. 51, no. 6, pp. 1721–1737, 2011.
- [11] R. E. A. Arndt, “Cavitation in Fluid Machinery and Hydraulic Structures,” *Annu. Rev. Fluid Mech.*, vol. 13, pp. 273–328, 1981.
- [12] M. J. Bloxham and J. P. Bons, “A Global Approach to Turbomachinery Flow Control: Passage Vortex Control,” *J. Turbomach.*, vol. 136, no. 4, p. 41003, 2013.
- [13] K. J. Farrell and M. L. Billet, “A Correlation of Leakage Vortex Cavitation in Axial-Flow Pumps,” *J. Fluids Eng.*, vol. 116, no. 3, p. 551, 1994.
- [14] F. J. G. Heyes, H. P. Hodson, and G. M. Dailey, “The Effect of Blade Tip Geometry on the Tip Leakage Flow in Axial Turbine Cascades,” *J. Turbomach.*, vol. 114, no. 3, pp. 643–651, 1992.
- [15] H. Wu, R. L. Miorini, and J. Katz, “Measurements of the tip leakage vortex structures and turbulence in the meridional plane of an axial water-jet pump,” *Exp. Fluids*, vol. 50, no. 4, pp. 989–1003, 2011.
- [16] M. I. Yaras and S. a. Sjolander, “Prediction of Tip-Leakage Losses in Axial Turbines,” *J. Turbomach.*, vol. 114, no. 1, p. 204, 1992.
- [17] C. Camci, D. Dey, and L. Kavurmacioglu, “Aerodynamics of Tip Leakage Flows Near Partial Squealer Rims in an Axial Flow Turbine Stage,” *J. Turbomach.*, vol. 127, no. 1, p. 14, 2005.

- [18] B. Lakshminarayana, *Fluid Dynamics and Heat Transfer of Turbomachinery*. New York, NY: John Wiley & Sons Inc., 1996.
- [19] J. P. Bindon, “The Measurement and Formation of Tip Clearance Loss,” *J. Turbomach.*, vol. 111, no. 3, p. 257, 1989.
- [20] J. Pu, J. Yu, J. Wang, W. Yang, Z. Zhang, and L. Wang, “An experimental investigation of secondary flow characteristics in a linear turbine cascade with upstream converging slot-holes using TR-PIV,” *Exp. Therm. Fluid Sci.*, vol. 59, pp. 56–71, 2014.
- [21] D. K. Van Ness II, T. C. Corke, and S. C. Morris, “Tip Clearance Flow Visualization of a Turbine Blade,” *ASME Turbo Expo*, 2008.
- [22] S. W. Lee and S. U. Kim, “Tip gap height effects on the aerodynamic performance of a cavity squealer tip in a turbine cascade in comparison with plane tip results: Part 1-tip gap flow structure,” *Exp. Fluids*, vol. 49, no. 5, pp. 1039–1051, 2010.
- [23] C. Prakash, C. P. Lee, D. G. Cherry, R. Doughty, and a. R. Wadia, “Analysis of Some Improved Blade Tip Concepts,” *J. Turbomach.*, vol. 128, no. 4, p. 639, 2006.
- [24] C. Zhou, H. Hodson, I. Tibbott, and M. Stokes, “Effects of Winglet Geometry on the Aerodynamic Performance of Tip Leakage Flow in a Turbine Cascade,” *J. Turbomach.*, vol. 135, no. 5, p. 51009, 2013.
- [25] S. W. Lee, S. U. Kim, and K. H. Kim, “Aerodynamic performance of winglets covering the tip gap inlet in a turbine cascade,” *Int. J. Heat Fluid Flow*, vol. 34, pp. 36–46, 2012.
- [26] Y. Il Yun, L. Porreca, A. I. Kalfas, S. Jin Song, and R. S. Abhari, “Investigation of Three-Dimensional Unsteady Flows in a Two-Stage Shrouded Axial Turbine Using Stereoscopic PIV—Kinematics of Shroud Cavity Flow,” *J. Turbomach.*, vol. 130, no. 1, p. 11021, 2008.

- [27] J. Hu, X. Kong, Z. Li, Y. Zhang, and J. Xu, "Experimental investigation of aerodynamic interaction between tip leakage flow and spontaneous tip injection flow using 2D-PIV," *Exp. Therm. Fluid Sci.*, vol. 54, pp. 127–135, 2014.
- [28] T. A. Auxier, "Aerodynamic tip sealing for rotor blades," US Patent No: US5403158 A, 1993.
- [29] Y. Ostovan, "Experimental Investigation of Waveform Tip Injection on the Characteristics of the Tip Vortex," Middle East Technical University, 2011.
- [30] H. M. El-Batsh, "Effect of the Radial Pressure Gradient on the Secondary Flow Generated in an Annular Turbine Cascade," vol. 2012, no. MArch, p. 14, 2012.
- [31] T. Matsunuma, "Effects of Reynolds Number and Free-Stream Turbulence on Turbine Tip Clearance Flow," *ASME Conf. Proc.*, vol. 2005, no. 47306, pp. 389–401, 2005.
- [32] A. M. Yocum and A. L. Treaster, "The Calibration And Application Of Five-Hole Probes," Pennsylvania, 1978.
- [33] A. Moscardi, "Five Hole Pressure Probe For Local Inflow Study On A Horizontal Axis," Politecnico Di Milano / University Of Waterloo, 2014.
- [34] A. Yamamoto and H. Nouse, "Effects of Incidence on Three-Dimensional Flows in a Linear Turbine Cascade," *J. Turbomach.*, vol. 110, no. October, pp. 486–496, 1988.
- [35] A. Yamamoto, "Interaction mechanisms between tip leakage flow and the passage vortex in a linear turbine rotor cascade," *J. Turbomach.*, vol. 110, no. 3, pp. 329–338, 1988.
- [36] Y. C. Nho, J. S. Park, Y. J. Lee, and J. S. Kwak, "Effects of turbine blade tip shape on total pressure loss and secondary flow of a linear turbine cascade," *Int. J. Heat Fluid Flow*, vol. 33, no. 1, pp. 92–100, 2012.

- [37] S. A. Sjolander, K. K. Amrud, and R. J. Kind, "Effects of Tip Clearance on Blade Loading in a Planar Cascade of Turbine Blades - Part II: Downstream Flow Field and Blade Loading," *J. Turbomach.*, vol. 109, no. 2, p. 237, 1991.

APPENDIX A

DATA PROCESSING OF FHP

The MatLab code used for creating calibration map and processing the measurement data of FHP is given below.

```
clear all
clc
% input calibration data
calraw=importdata ('raw1 - Kopya.txt');
yaw_cal=calraw(:,1);
pitch_cal=calraw(:,2);
p1c=calraw(:,3);
p2c=calraw(:,4);
p3c=calraw(:,5);
p4c=calraw(:,6);
p5c=calraw(:,7);
pmeanc=(p2c+p3c+p4c+p5c)/4;
cpy=(p2c-p3c)/(p1c-pmeanc);
cpp=(p5c-p4c)/(p1c-pmeanc);
```

```

cpt=(p1c-794.6144)./(p1c-pmeanc);
cps=(pmeanc-37.6188)./(p1c-pmeanc);

% calmat=[yaw_cal pitch_cal cpy cpp cpt cps];

% input measurement data
meas_raw=importdata('meas_raw.txt');
pos_x=meas_raw(:,1);
pos_y=meas_raw(:,2);
p1=meas_raw(:,3);
p2=meas_raw(:,4);
p3=meas_raw(:,5);
p4=meas_raw(:,6);
p5=meas_raw(:,7);
pmean=(p2+p3+p4+p5)/4;
cpyn=(p2-p3)./(p1-pmean);
cppn=(p5-p4)./(p1-pmean);

% prompt1 = 'What is the yaw_cp value? ';
% cpyn = input(prompt1);
% prompt2 = 'What is the pitch_cp value? ';
% cppn = input(prompt2);

yaw_n = griddata(cpp,cpy,yaw_cal,cppn,cpyn,'v4');
pitch_n = griddata(cpp,cpy,pitch_cal,cppn,cpyn,'v4');
cpt_n = griddata(cpp,cpy,cpt,cppn,cpyn,'v4');

```

```

cpsn = griddata(cpp,cpy,cps,cppn,cpyn,'v4');

rho=1.07258;

dp=p1-pmean;
% dcp=abs(cptn-cpsn);
ptn=p1-(cptn.*dp);
psn=pmean-(cpsn.*dp);
vel=sqrt((2/rho)*(ptn-psn));
% scatter (cpp,cpy,'filled');
% title('cpy vs. cpp calibration');
% xlabel('Pitch Cp') % x-axis label
% ylabel('Yaw Cp') % y-axis label
% hold on
% xh = [-4 4]; yh = [cppn cppn];
% xv = [cpyn cpyn]; yv = [-4 4];
% plot(xh,yh,xv,yv)

result = [pos_x,pos_y,ptn,psn,yawn,pitchn,vel];

% fid = fopen('result.txt', 'w');
% fprintf(fid, '%4.2f %4.2f %6.3f %6.3f %6.3f', result);
% fclose(fid);
-----

```

APPENDIX B

UNCERTAINTY CALCULATIONS

For FHP and Kiel probe measurements, 300 samples were taken at each point. Then, the average of these values was labeled as the value of that point. This procedure is applied for all collected data. After this point, data is processed according to the probe used to collect it.

In here, an uncertainty calculation will be given as an example on the data of FHP. The pressure transducer used (Scanivalve DSA3217) has $\pm 0,4$ full scale accuracy and ± 2895 Pa full scale range. Error margin of each pressure reading is constant and $\pm 11,58$ Pa. A sample of FHP calibration data is given in Table B.1 for using in calculations.

Table B. 1: An example of FHP calibration data

Yaw angle	Pitch angle	P1 (Pa) + Δe	P2 (Pa) + Δe	P3 (Pa) + Δe	P4 (Pa) + Δe	P5 (Pa) + Δe
0	0	758,5101 \pm 11,58	288,4227 \pm 11,58	287,8752 \pm 11,58	284,5606 \pm 11,58	285,4344 \pm 11,58

In calibration phase, Cp coefficients were calculated according to the formulas given below.

$$C_{p,yaw} = \frac{P_2 - P_3}{P_1 - \bar{P}}, \quad C_{p,pitch} = \frac{P_5 - P_4}{P_1 - \bar{P}}$$

$$C_{p,tot} = \frac{P_1 - P_{tot}}{P_1 - \bar{P}}, \quad C_{p,st} = \frac{\bar{P} - P_{st}}{P_1 - \bar{P}}$$

$$\bar{P} = \frac{P_2 + P_3 + P_4 + P_5}{4}$$

The calculated values and errors are given in the Table B.2 below.

Table B. 2: Average and absolute error values of FHP coefficients

	Cp,yaw	Cp,pitch	Cp,tot	Cp,st
Average value	0,0012	0,0019	-0,0765	0,5275
Absolute error	+/-0,0347	+/-0,0347	+/-0,0348	+/-0,0392

After calibration phase, the measurements were carried out and a set of values belong to a certain point is given in Table B.3. And according to these values, Cp coefficients were calculated and given in Table B.4.

Table B. 3: An example of data acquired from measurements

Pitchwise Coordinate	Spanwise Coordinate	P1 (Pa) + Δe	P2 (Pa) + Δe	P3 (Pa) + Δe	P4 (Pa) + Δe	P5 (Pa) + Δe
35	240	687,463 +/-11,58	274,501 +/-11,58	234,653 +/-11,58	207,761 +/-11,58	284,544 +/-11,58

Table B. 4: Average and absolute error values of FHP coefficients

	Cp,yaw	Cp,pitch	Cp,tot	Cp,st
Average value	0,0912	0,1757	-0,2451	0,4867
Absolute error	+/-0,0376	+/-0,0380	+/-0,0386	+/-0,0417

From pressure values found in data acquisition, a reverse calculation was done to find the total and static pressures using the Cp values read from calibration map. The result of uncertainty levels are given at Table B.5. If these Cp values found from measurements did not coincide with the any points on calibration map, bicubic interpolation is done which is a complex and advanced procedure and analysis is beyond the scope of this work.

Table B. 5: Uncertainties of total / static pressures and velocity measurement

	Calculated Values	Uncertainty	Percentage
Pt	794,6144 Pa	+/-11,5805	1,45%
Pst	474,7171 Pa	+/-11,5802	2,44%
Velocity	24,4186 m/s	+/-0,3353	1,37%

As can be seen from the Table B.5, all error levels are less than 2,5%. The uncertainty is more in static pressure measurements and C_p coefficients, since the uncertainty level of the pressure transducer is given relative to full scale range of the device. This means that this device is suitable for our measurement levels and measuring larger values (in the order of hundreds of Pa).

APPENDIX C

FHP DATA PROCESSING PROCEDURE

In Appendix B, a short calculation phase of FHP data is given. The calibration and processing of measured data sequence is written as listed below.

- The FHP is located at the middle of the calibration jet.
- Calibration jet is set to produce desired velocity level. This velocity is obtained from the measurement plane.
- Probe is rotated at desired pitch and yaw angle combinations.
- The measured pressure data are converted into C_p values. ($C_{p,yaw}$ vs $C_{p,pitch}$ graph)
- After data are acquired from the measurement plane, $C_{p,yaw}$ and $C_{p,pitch}$ values are calculated and the correspondent angle combination is found in calibration map. The angle pair found relative to these coefficients gives the direction of the flow at that point.
- With using $C_{p,tot}$ and $C_{p,st}$, total and static pressures, and in turn the magnitude of the velocity at that point is found.
- Using the angles found, velocity components are calculated.

For further information and formulas about the calibration and data processing process, Treaster and Yocum [32] is a useful and clear guide.